Renormalization of quark propagators from twisted-mass lattice QCD at $N_f = 2$

B. Blossier,[1] Ph. Boucaud,[1] M. Brinet,[2] F. De Soto,[3] Z. Liu,[4,5] V. Morenas,[6] O. Pène,[1] K. Petrov,[1] and J. Rodríguez-Quintero[7]

[1]*Laboratoire de Physique Théorique*[*]*, CNRS, and Université Paris-Sud XI, Bâtiment 210, 91405 Orsay Cedex, France*
[2]*Laboratoire de Physique Subatomique et de Cosmologie, CNRS/IN2P3/UJF, 53 avenue des Martyrs, 38026 Grenoble, France*
[3]*Departamento Sistemas Físicos, Químicos y Naturales, Universidad Pablo de Olavide, 41013 Sevilla, Spain*
[4]*DAMTP, University of Cambridge, Wilberforce Road, Cambridge CB3 0WA, United Kingdom*
[5]*Institute of High Energy Physics, Chinese Academy of Science, Beijing 100049, China*
[6]*Laboratoire de Physique Corpusculaire, Université Blaise Pascal, CNRS/IN2P3, 63177 Aubière Cedex, France*
[7]*Departamento Física Aplicada, Facultad Ciencias Experimentales, Universidad de Huelva, 21071 Huelva, Spain*

(Received 13 November 2010; published 20 April 2011)

We present results concerning the nonperturbative evaluation of the renormalization constant for the quark field, Z_q, from lattice simulations with twisted-mass quarks and three values of the lattice spacing. We use the regularization-invariant momentum-subtraction (RI'-MOM) scheme. Z_q has very large lattice spacing artefacts; it is considered here as a test bed to elaborate accurate methods which will be used for other renormalization constants. We recall and develop the nonperturbative correction methods and propose tools to test the quality of the correction. These tests are also applied to the perturbative correction method. We check that the lattice-spacing artefacts indeed scale as a^2p^2. We then study the running of Z_q with particular attention to the nonperturbative effects, presumably dominated by the dimension-two gluon condensate $\langle A^2\rangle$ in Landau gauge. We show indeed that this effect is present, and not small. We check its scaling in physical units, confirming that it is a continuum effect. It gives a $\sim$4% contribution at 2 GeV. Different variants are used in order to test the reliability of our result and estimate the systematic uncertainties. Finally, combining all our results and using the known Wilson coefficient of $\langle A^2\rangle$, we find $g^2(\mu^2)\langle A^2\rangle_{\mu^2\mathrm{CM}} = 2.01(11)(^{+0.61}_{-0.73})\mathrm{GeV}^2$ at $\mu = 10$ GeV, the local operator A^2 being renormalized in the $\overline{\mathrm{MS}}$ scheme. This last result is in fair agreement within uncertainties with the value independently extracted from the strong coupling constant. We convert the nonperturbative part of Z_q from the regularization-invariant momentum-subtraction (RI'-MOM) scheme to $\overline{\mathrm{MS}}$. Our result for the quark field renormalization constant in the $\overline{\mathrm{MS}}$ scheme is $Z_q^{\overline{\mathrm{MS}}\mathrm{pert}}((2\,\mathrm{GeV})^2, g^2_{\mathrm{bare}}) = 0.750(3)(7) - 0.313(20)(g^2_{\mathrm{bare}} - 1.5)$ for the perturbative contribution and $Z_q^{\overline{\mathrm{MS}}\mathrm{nonperturbative}}((2\,\mathrm{GeV})^2, g^2_{\mathrm{bare}}) = 0.781(6)(21) - 0.313(20)(g^2_{\mathrm{bare}} - 1.5)$ when the nonperturbative contribution is included.

DOI: 10.1103/PhysRevD.83.074506 PACS numbers: 12.38.Gc, 11.15.Ha, 12.38.Aw, 12.38.Cy

I. INTRODUCTION

Computing matrix elements in lattice quantum chromodynamics (LQCD) often needs the computation of renormalization constants. Indeed, even if the lattice computation contains only $O(a^2)$ lattice artefacts, the bare quantities differ from the continuum ones by $O(g^2) \simeq O(1/\log(a^2))$, which is unacceptable. Renormalization restores the $O(a^2)$ accuracy. It has also been known for a long time that these renormalization constants need to be computed nonperturbatively, using LQCD techniques.

Several nonperturbative methods have been proposed. Let us here concentrate on those based on the MOM scheme. They start from the computation of Green functions of quarks, gluons, and ghosts at large enough momenta in a fixed gauge, usually the Landau gauge. This gives the renormalization constant $Z(\mu)$ at many values of the scale μ. Assuming that our goal is to deliver the renormalization constant in the $\overline{\mathrm{MS}}$ scheme at, say, 2 GeV (a typical phenomenological scale), one must then use results from perturbative QCD to convert MOM into $\overline{\mathrm{MS}}$ and run to 2 GeV. The running of $Z_{\mathrm{MOM}}(\mu)$ is a very powerful testing tool: indeed, perturbative QCD is only useful if we are in the perturbative regime, i.e., at large enough momenta. The only way to check whether this is the case is to compare lattice data with the perturbative running. In this framework, it turns out that this is not always the case.

Deviations from perturbative running can be analyzed via Wilson operator expansion and the Shifman-Vainshtein-Zakharov sum rules. It turns out that the dominant nonperturbative correction in Landau gauge is due to the nonvanishing vacuum expectation value of the only dimension-two operator: $A^2 \equiv A^a_\mu A^{a\mu}$ [1], and that it is not small [2–8]. It is thus necessary to carefully look for the possibility of such a contribution, which appears in the operator product expansion (OPE), as a $1/p^2$ contribution up to logarithmic corrections. The coefficient of this $1/p^2$ contribution is equal to the vacuum expectation value

[*]Unité Mixte de Recherche 8627 du Centre National de la Recherche Scientifique

$g^2\langle A^2\rangle$ times a Wilson coefficient that has to be computed in perturbation theory, and has been up to three loops for propagators [9]. To argue that a measured $1/p^2$ contribution is a continuum power correction and not a lattice artefact, we must check that the $1/p^2$ term in the fit scales with lattice spacing when expressed *in physical units*. To further argue that this is indeed due to $\langle A^2\rangle$, we must compare the resulting $\langle A^2\rangle$ from different quantities and thus check the universality of the condensates which is based on the Shifman-Vainshtein-Zakharov technology. The theory of Wilson operator expansion is then constraining: since there exists only one dimension-two operator, provided that it is renormalized with the same prescription for all these quantities, all the different estimates of $\langle A^2\rangle$ should coincide within errors, up to $1/p^4$ corrections, for a given value of N_f and of the dynamical masses. Of course, its extraction needs the coefficients of the Wilson expansion which are computable in perturbation. To test this universality of the extracted $\langle A^2\rangle$ is one of the goals of our program of analyzing many different quark and gluon quantities obtained from lattice gauge configurations produced by the European Twisted Mass Collaboration (ETMC). We have also applied a criterion proposed in [10] to validate the way we use operator expansion. This paper takes one of the first steps in such a program.

It is worthwhile also to mention that several authors have elaborated further on the relation between this gauge-dependent gluon condensate, obtained in the Landau gauge, and possible $1/p^2$-terms in gauge invariant quantities, and thus on the phenomenological implications, mainly in connection with confinement scenarios, of such a dimension-two condensate [11].

All this can only be done once the lattice artefacts are eliminated or at least under control. The $O(a^2)$ artefacts can be quite large since we consider large momenta, while finite volume artefacts are minor. There are two main types of $O(a^2)$ artefacts: $O(a^2p^2)$ artefacts, which respect the continuum $O(4)$ rotation symmetry, and hypercubic artefacts, which respect the $H(4)$ hypercubic symmetry group but not $O(4)$. The latter are effects of the hypercubic symmetry of the lattice action. We will identify the $O(a^2p^2)$ artefacts nonperturbatively by doing a fit of the running $Z(\mu)$, which will include the perturbative running, the $\langle A^2\rangle$ power correction, and a term proportional to a^2p^2. Notice that, while the perturbative and $\langle A^2\rangle$ running contributions must approximately scale in physical units, the artefacts must scale in lattice units. This is an additional check we shall perform.

Concerning the elimination of hypercubic artefacts, which is better done before the above-mentioned running fit, several methods have been proposed in literature: the democratic selection, the perturbative correction, and the nonperturbative ''egalitarian'' one (''egalitarian'' because all the points are used on the same footing in this approach). We will discuss this in some detail later and perform extensive comparisons. In particular, we will use a new quality test which consists of watching to what extent the ''half-fishbone'' structure, which raw lattice results for Z_q always exhibit and which is a dramatic illustration of hypercubic artefacts, are corrected by every method.

Although all the issues raised here concern all the renormalization constants as well as the QCD coupling constant, we will concentrate in the following on Z_q that renormalizes the quark field,

$$q_R = Z_q^{1/2} q_B, \tag{1.1}$$

where q_B (q_R) is the bare (renormalized) quark field. In the regularization-invariant momentum-subtraction (RI'-MOM) scheme, Z_q is defined by

$$Z_q(\mu^2 = p^2) = \frac{-i}{12p^2}\,\mathrm{Tr}[S_{\mathrm{bare}}^{-1}(p)\not{p}], \tag{1.2}$$

where $S_{\mathrm{bare}}(p)$ is the bare quark propagator. Our goal is to compute that constant from LQCD with twisted Wilson quarks.

In [4,12], a study[1] of Z_q was performed from LQCD in the case $N_f = 0$ using both the overlap and Wilson clover fermions. In [12], the exceptional size of hypercubic artefacts was stressed and a nonperturbative elimination of hypercubic artefacts was performed along the same principle as we use here. In [4], the Wilson coefficient of the $\langle A^2\rangle$ was computed up to the leading logarithm approximation and applied to estimate the condensate from the LQCD data. The outcome was that a significant nonperturbative contribution from $\langle A^2\rangle$ was needed to account for the results. Notice that we do not expect the $\langle A^2\rangle$ to be similar or even close in the cases of $N_f = 0$ and $N_f = 2$.

Summarizing the above discussion, we do here concentrate on Z_q because we consider it as a kind of benchmark for the following reasons:

(a) It has especially large hypercubic artefacts and is thus a good test bed for a correct treatment of these.
(b) It has a vanishing anomalous dimension at leading order in the Landau gauge: its perturbative running is thus soft.
(c) The Wilson coefficient of the $\langle A^2\rangle$ condensate is rather large [4,9], which is an incentive to look carefully for nonperturbative contributions.

In this paper, in order to test deeply the reliability of our results, we will compare many fits: perturbative/nonperturbative hypercubic correction, one-window/sliding-windows nonperturbative hypercubic correction, effect of the total fitting range, fitting separately every β, and global fit. As a consequence, we will proceed as follows:

[1] In [4], Z_q was denoted Z_ψ.

(a) Recall some general formulae concerning the perturbative and nonperturbative running in the continuum;
(b) Describe our lattice setting and our nonperturbative egalitarian method to eliminate hypercubic artefacts;
(c) Present the results concerning the *perturbative* correction method for hypercubic artefacts and show the quality checks;
(d) Present the results concerning the *nonperturbative* method to correct for hypercubic artefacts, show the quality checks, and propose two types of fits, the sliding-windows fit (SWF) and the one-window fit (OWF);
(e) Perform the running fit on the output of all of the previously mentioned hypercubic corrected data, compare the results for the $g^2\langle A^2\rangle$ for all these fits, and check the scaling of $g^2\langle A^2\rangle$;
(f) Check the scaling of the $\propto a^2p^2$ artefacts;
(g) Check the lattice spacing dependence of $Z_q^{\rm pert}$, the perturbative contribution to Z_q, $\propto g^2$;
(h) Study the range of variation of our results for $g^2\langle A^2\rangle$ from the egalitarian method with one window/sliding-windows, with varying fitting ranges, and the perturbative method with two realizations, and extract from there the systematic uncertainty;
(i) Join in one plot the three β's and perform the fit of the running;
(j) Compare the resulting $g^2\langle A^2\rangle$ with the one extracted from the strong coupling constant and with quenched estimates, and test our procedure according to Martinelli-Sachrajda's criterion [10];
(k) Conclude.

II. RUNNING OF Z_q

A. Perturbative running

In Landau gauge, Z_q has a vanishing anomalous dimension to leading order, i.e., its running starts at $O(\alpha^2)$. The perturbative running has been computed up to four loops (see [13] and references therein). The needed formulae are accessible on the web site in Ref. [13].

B. Wilson expansion and nonperturbative running

To handle nonperturbative corrections, we use the theory of operator product expansion [14] and its application in estimating power-suppressed nonperturbative corrections via vacuum expectation values [15]. In Landau gauge, there exists only one dimension-two operator allowed to have a vacuum expectation value: $A^2 \equiv \sum_{\mu=1,4}^{a=1,8} A_\mu^a A^{a\mu}$. The Wilson coefficient of this operator has been computed to leading logarithm in [4] and extensively for all propagators up to $O(\alpha^4)$ in [9].

1. $\langle A^2\rangle$ tree-level Wilson coefficients for Z_q

In order to give a hint, let us just sketch the tree-level calculation of that Wilson coefficient.

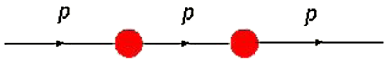

Consider the above diagram describing a quark propagating in a constant background gauge field. As a consequence the [red] filled bubbles represent the interaction of the quark with this background field: $ig\lambda_a/2A^a$. The Feynman rules are then applied as usual. Neglecting the quark mass, it gives

$$\frac{-i\not p}{p^2}\left(\sum_{\mu=1,a=1}^{\mu=4,a=8}\sum_{\mu'=1,a'=1}^{\mu'=4,a'=8} ig\frac{\lambda_a}{2}A_\mu^a\gamma^\mu\frac{-i\not p}{p^2}ig\frac{\lambda_{a'}}{2}A_{\mu'}^{a'}\gamma^{\mu'}\delta_{aa'}\delta_{\mu\mu'}\right)\frac{-i\not p}{p^2} = -\frac{g^2}{12}\frac{\langle A^2\rangle}{p^2}\times\frac{-i\not p}{p^2}, \tag{2.1}$$

where $\langle\,\rangle$ represents the vacuum expectation value, $\sum\lambda_a^2/4 = C_F = 4/3$ (proportional to the identity matrix in color space), the sum over μ gives a factor 4, and

$$\langle(A_\mu^a)^2\rangle = \langle A^2/32\rangle, \qquad \langle(A\cdot\hat p)^2\rangle = \langle A^2/4\rangle \tag{2.2}$$

from the homogeneity of the vacuum for rotations in spacetime and color space.

For Z_q defined by Eq. (1.2), we get at tree level the following nonperturbative contribution due to $\langle A^2\rangle$:

$$\delta Z_q = \frac{g^2}{12}\frac{\langle A^2\rangle}{p^2}. \tag{2.3}$$

2. The Wilson coefficients at $O(\alpha^4)$

The Wilson coefficient of $\langle A^2\rangle$ for the quark propagator has been computed up to $O(\alpha^4)$ in [9] in the $\overline{\rm MS}$ scheme. Our lattice data refer naturally to the RI'-MOM scheme. Some work is needed to derive the correct analytic formula which allows a fitting of our lattice data. We have derived this in the Appendix.

III. THE LATTICE COMPUTATIONS

The results presented here are based on the gauge field configurations generated by the European Twisted Mass Collaboration (ETMC) with the tree-level improved Symanzik gauge action [16] and the twisted mass fermionic action [17] at maximal twist.

A. The lattice action

A very detailed discussion about the twisted mass and tree-level improved Symanzik gauge actions, and about the way they are implemented by ETMC, can be found in Refs. [18–21]. Here, for the sake of completeness, we will present a brief reminder of the twisted action and the run parameters for the gauge configurations that will be exploited in the present work (see Table I.)

The Wilson twisted mass fermionic lattice action for two flavors of mass degenerate quarks reads (in the so-called twisted basis [17,22])

$$\begin{aligned} S^{\mathrm{F}}_{\mathrm{tm}} &= a^4 \sum_x \{\bar{\chi}_x [D_{\mathrm{W}} + m_0 + i\gamma_5 \tau_3 \mu_q] \chi_x\}, \\ D_{\mathrm{W}} &= \frac{1}{2}\gamma_\mu (\nabla_\mu + \nabla^*_\mu) - \frac{ar}{2}\nabla_\mu \nabla^*_\mu, \end{aligned} \tag{3.1}$$

where m_0 is the bare untwisted quark mass and μ_q the bare twisted quark mass, τ_3 is the third Pauli matrix acting in flavor space, and r is the Wilson parameter, which is set to $r = 1$ in the simulations. The twisted Dirac operator is defined as

$$D_{\mathrm{tw}} \equiv D_{\mathrm{W}} + m_0 + i\gamma_5 \tau_3 \mu_q. \tag{3.2}$$

The operators ∇_μ and ∇^*_μ stand for the gauge covariant nearest neighbor forward and backward lattice derivatives:

$$\begin{aligned} \nabla_\mu(x, y) &\equiv [\delta_{y,x+\hat{\mu}} U_\mu(x) - \delta_{x,y}], \\ \nabla^\star_\mu(x, y) &= [\delta_{x,y} - \delta_{y,x-\hat{\mu}} U^\dagger_\mu(x - \hat{\mu})], \\ D_\mu &\equiv \frac{1}{2}[\nabla_\mu(x, y) + \nabla^\star_\mu(x, y)] \\ &= \frac{1}{2}[\delta_{y,x+\hat{\mu}} W(x, y) - \delta_{y,x-\hat{\mu}} W(x, y)], \end{aligned} \tag{3.3}$$

defining the operator D_μ as the discretized covariant derivative. The bare quark mass m_0 is related as usual to the so-called hopping parameter κ, by $\kappa = 1/(8 + 2am_0)$. Twisted mass fermions are said to be at *maximal twist* if the bare untwisted mass is tuned to its critical value, m_{crit}. This is in practice done by setting the so-called untwisted partially conserved axial current (PCAC) mass to zero.

In the gauge sector, the tree-level Symanzik improved gauge action (tlSym) [16] is applied. This action also includes, besides the plaquette term $U^{1\times1}_{x,\mu,\nu}$, rectangular (1×2) Wilson loops $U^{1\times2}_{x,\mu,\nu}$. It reads

TABLE I. Run parameters of the exploited data from the ETMC Collaboration for the present study of Z_q. The second column lists the lattice spacings which we have used in this study.

β	a fm	a^{-1} GeV	$a\mu_q$	Volume	# confs
3.9	0.083	2.373	0.004	$24^3 \times 48$	100
4.05	0.0675	2.897	0.006	$24^3 \times 48$	100
4.2	0.055	3.58	0.002	$24^3 \times 48$	100

$$\begin{aligned} S_g = \frac{\beta}{3}\sum_x \Big(b_0 \sum_{\mu,\nu=1 1\le\mu<\nu}^{4} \{1 - \mathbb{R}\mathrm{e}\,\mathrm{Tr}(U^{1\times1}_{x,\mu,\nu})\} \\ + b_1 \sum_{\mu,\nu=1\mu\neq\nu}^{4} \{1 - \mathbb{R}\mathrm{e}\,\mathrm{Tr}(U^{1\times2}_{x,\mu,\nu})\} \Big), \end{aligned} \tag{3.4}$$

where $\beta \equiv 6/g_0^2$, g_0 being the bare lattice coupling, and it is set $b_1 = -1/12$ (with $b_0 = 1 - 8b_1$ as dictated by the requirement of continuum limit normalization). Note that, at $b_1 = 0$, this action becomes the usual Wilson plaquette gauge action. The run parameters for β and μ_q of the gauge configurations that will be exploited in the following can be found in Table I.

B. The computation of the quark propagator

Computing the renormalization constants for the quark propagator and the operators containing quark fields demands that we first compute the gauge-fixed two-point quark Green functions from the lattice. We exploited ETMC gauge configurations [23] obtained for $\beta = 3.9$, $\beta = 4.05$, and $\beta = 4.2$. After checking the small dependence of Z_q on the dynamical and valence quark masses, we decided to use only one mass for every β (Table I). The lattice gauge configurations are transformed to Landau gauge by minimizing the following functional of the SU (3) matrices, $U_\mu(x)$,

$$F_U[g] = \mathrm{Re}\Big[\sum_x \sum_\mu \mathrm{Tr}\Big(1 - \frac{1}{N} g(x) U_\mu(x) g^\dagger(x + \mu)\Big)\Big], \tag{3.5}$$

with respect to the gauge transform g, by applying a combination of overrelaxation algorithm and Fourier acceleration.[2]

We compute quark propagators with a local source on gauge configurations separated by 20 trajectories in order to have them decorrelated.[3] To be even safer, we take the source at a random point x_0 on the lattice during the inversion:

$$\begin{aligned} S(y, x_0)^{a,\alpha;b_0,\beta_0}_i &= D^{-1}_{\mathrm{tw}}(y, x)^{a,\alpha;b,\beta;i,j} so^{b,\beta}_j(x, x_0), \\ so^{b,\beta}_j(x, x_0) &= \delta_{x,x_0}\delta_{b,b_0}\delta_{\beta,\beta_0}, \end{aligned} \tag{3.6}$$

where the equation is solved for every $b_0 = 1, 3$ and $\beta_0 = 1, 4$, and $j = u, d$ labels the isospin. The aim of taking a random source is to prevent that the inversion of all the

[2]We end when $|\partial_\mu A_\mu|^2 < 10^{-11}$ and when the spatial integral of A_0 is constant in time to better than 10^{-6}.

[3]As explained in Ref. [23], at least 1500 trajectories for equilibration were allowed in generating the configurations analyzed here and, as can be seen in Table 2 of Ref. [23], some integrated autocorrelation time checks were applied to these configurations and clearly indicate their decorrelation. We also confirmed directly the decorrelation for a sample of our configurations by computing the time correlation function for the propagators with either fixed or random point sources.

configurations with the same fixed point for the source might introduce some new correlations. We perform the Fourier transform, which is a 12×12 complex matrix:

$$S_i(p) \equiv \sum_y e^{-ip(y-x_0)} S_i(y, x_0). \tag{3.7}$$

This is the Fourier transform of the quark incoming to the source (the arrow pointing towards the source). The Fourier transform of the quark outgoing from the source is

$$S_i^{\dagger 5}(p) = \gamma_5 S_i^\dagger(p) \gamma_5, \tag{3.8}$$

where $\bar{u} \equiv d$; $\bar{d} \equiv u$. From Eq. (1.2), the lattice quark renormalization constant Z_q is given by

$$Z_q(p) \equiv \frac{-i}{12\tilde{p}^2} \langle \mathrm{Tr}[S^{-1}(p)\tilde{p}] \rangle, \tag{3.9}$$

where $<\ldots>$ means here the average over the chosen ensemble of thermalized configurations and $\tilde{p}_\mu = \frac{1}{a} \times \sin a p_\mu$. The reason for using $\tilde{p}_\mu = \frac{1}{a} \sin a p_\mu$ is to get $Z_q = 1$ for a free fermion, or, in other words, to eliminate hypercubic artefacts at tree level.

C. The method of nonperturbative hypercubic $H(4)$ correction

The lattice estimates of the quark field renormalization constant and the vertex functions lead to dimensionless quantities that, because of general dimensional arguments, depend on the strong interaction scale Λ_{QCD} and on the lattice momentum $a p_\mu$. We have computed the Fourier transforms for the following momenta:

$$\begin{aligned} p_i &= \frac{2\pi n_i}{N_L a} \qquad n_i = -N_L/4, \cdots, N_L/4, \\ p_4 &= \frac{\pi(2n_4+1)}{N_T a} \qquad n_4 = -N_T/4, \cdots, N_T/4, \end{aligned} \tag{3.10}$$

where $p_i = 1, 3$ are the spatial momenta and p_4 the timelike ones. The antiperiodic boundary condition in the time direction explains the $\pi(2n_4 + 1)$ factor.

The lattice action Eqs. (3.1) and (3.4) is invariant under the hypercubic group $H(4)$. However, the boundary conditions and the difference between the spatial size N_L and the timelike one $N_T = 2N_L$ generate finite volume corrections to the hypercubic symmetry. Only the cubic symmetry is exact. We define cubic invariant quantities and compute their average over the cubic group. We have thus a set of measures for every orbit of the cubic group, labeled by

$$\left(\sum_{i=1,3} p_i^m, p_4 \right), \tag{3.11}$$

where $m = 2, 4, 6$.

The first kind of artefacts that can be systematically cured [12,24,25] are those due to the breaking of the rotational symmetry of the Euclidean space-time when using a hypercubic lattice, where this symmetry is restricted to the discrete hypercubic $H(4)$ isometry group. However, as already mentioned, we also have finite volume effects which break $H(4)$. We therefore need to adapt the method. One idea could be to generalize it to a cubic symmetry. This happens not to be practical due to too few cubic symmetric orbits for a given $\vec{p}^{\,2}$. We choose another approach motivated by the fact that the lattice action is indeed $H(4)$ symmetric and that finite volume effects are expected to be small at large momenta compared to finite lattice spacing artefacts. We therefore use a slight variation of the method described in [24,25]: we apply it to the cubic orbits of Eq. (3.11), keeping track of p_4 which is not an $H(4)$ symmetric quantity.

Defining the $H(4)$ invariants to be

$$p^{[4]} = \sum_{\mu=1}^4 p_\mu^4, \quad p^{[6]} = \sum_{\mu=1}^4 p_\mu^6, \quad p^{[8]} = \sum_{\mu=1}^4 p_\mu^8, \tag{3.12}$$

it happens that every cubic orbit in Eq. (3.11) has a well-defined set of values for these $H(4)$ invariants, but several cubic orbits may have the same $H(4)$ invariants. We will neglect $p^{[8]}$, which plays no role on small lattices. We can thus define the quantity $Z_q(a p_\mu)$ averaged over the cubic orbits as

$$Z_q^{\mathrm{latt}}(a^2 p^2, a^4 p^{[4]}, a^6 p^{[6]}, a p_4, a^2 \Lambda_{\mathrm{QCD}}^2). \tag{3.13}$$

We expect the hypercubic effects to be $O(a^2)$ lattice artefacts and therefore to be expandable into powers of a^2. This would of course trivially be the case if $a^2 p^2 \ll 1$ since then, for example, $\epsilon = a^2 p^{[4]}/p^2 \le a^2 p^2 \ll 1$. (We take on purpose this quantity which will be seen to be dominant.) Then a Taylor expansion of Eq. (3.13) will ensure the artefact to be $O(a^2)$. However, aiming at measuring Z_q at large momentum, we go up to $a^2 p^2 \sim 3$–4. We will assume, and then check, that the Z_q^{latt} in Eq. (3.13) can be Taylor-expanded around $p^{[4]} = 0$ up to ϵ significantly larger than 1:

$$\begin{aligned} &Z_q^{\mathrm{latt}}(a^2 p^2, a^4 p^{[4]}, a^6 p^{[6]}, a p_4, a^2 \Lambda_{\mathrm{QCD}}^2) \\ &\quad = Z_q^{\mathrm{hyp_{corrected}}}(a^2 p^2, a p_4, a^2 \Lambda_{\mathrm{QCD}}^2) \\ &\qquad + R(a^2 p^2, a^2 \Lambda_{\mathrm{QCD}}^2) a^2 \frac{p^{[4]}}{p^2} + \cdots, \end{aligned} \tag{3.14}$$

where

$$R(a^2 p^2, a^2 \Lambda_{\mathrm{QCD}}^2) = \left. \frac{d Z_q^{\mathrm{latt}}(a^2 p^2, 0, 0, 0, a^2 \Lambda_{\mathrm{QCD}}^2)}{d\epsilon} \right|_{\epsilon=0}. \tag{3.15}$$

Of course, terms proportional to $p^{[6]}$, $p^{[4]2}$, etc., can be added analogously to the formula, as well as terms breaking $H(4)$. However, we have found that our data were not accurate enough to allow fitting them, and that using only

Eqs. (3.14) and (3.15) gave satisfactory fits. Now we must describe how we fit the functions appearing in the right-hand side (rhs) of Eq. (3.14).

1. The sliding-windows fit (SWF)

We consider all values of a^2p^2 in the range $a^2p^2_{\mathrm{min_{in}}} \le a^2p^2 \le a^2p^2_{\mathrm{max_{in}}}$, each of which contains a set of cubic orbits. We choose an integer width w (we will use $w = 10$ in numerical applications) and define a window as the set of $2w + 1$ values of a^2p^2 around an $a^2p^2_{\mathrm{center}}$ (w contiguous values below $a^2p^2_{\mathrm{center}}$ and as many above). There are as many windows as values of $a^2p^2_{\mathrm{center}}$ such that all of them are in the range $[a^2p^2_{\mathrm{min_{in}}}, a^2p^2_{\mathrm{max_{in}}}]$. This defines the range of interest $a^2p^2_{\mathrm{min_{out}}} \le a^2p^2_{\mathrm{center}} \le a^2p^2_{\mathrm{max_{out}}}$.

For every window, we use for the fit all cubic orbits corresponding to the values of a^2p^2 in the window. We fit, according to Eq. (3.14), $2w + 2$ parameters which are the $2w + 1$ values of $Z_q^{\mathrm{hyp_{corrected}}}(a^2p^2, a^2\Lambda^2_{\mathrm{QCD}})$ within the window, and one common value of $R(a^2p^2_{\mathrm{center}}, a^2\Lambda^2_{\mathrm{QCD}})$. The dependence in these parameters is linear, and thus the fit amounts to invert a matrix. It is clear that, for any a^2p^2, the $Z_q^{\mathrm{hyp_{corrected}}}(a^2p^2, a^2\Lambda^2_{\mathrm{QCD}})$ is fitted every time a^2p^2 is within a window, i.e., $2w + 1$ times. We keep as the final result only the result of the fit when a^2p^2 is the center of the window. At the end of the fit, for every $a^2p^2_{\mathrm{center}}$ in the range $a^2p^2_{\mathrm{min_{out}}} \le a^2p^2_{\mathrm{center}} \le a^2p^2_{\mathrm{max_{out}}}$ we have, as expected, a fitted value for both functions of the rhs of Eq. (3.14).

We can then study the function $R(a^2p^2, a^2\Lambda^2_{\mathrm{QCD}})$. As will be reported later (see, for instance, Fig. 6), we find that a reasonable approximation for R is

$$R(a^2p^2, a^2\Lambda^2_{\mathrm{QCD}}) = c_{a2p4} + c_{a4p4}a^2p^2. \tag{3.16}$$

This leads to the one-window fit.

2. The one-window fit (OWF)

We tune w such that only one window (or at worst two) is included in the range $[a^2p^2_{\mathrm{min_{in}}}, a^2p^2_{\mathrm{max_{in}}}]$. We then perform the fit for that window according to the equation

$$\begin{aligned} &Z_q^{\mathrm{latt}}(a^2p^2, a^4p^{[4]}, a^6p^{[6]}, ap_4, a^2\Lambda^2_{\mathrm{QCD}}) \\ &\quad = Z_q^{\mathrm{hyp_{corrected}}}(a^2p^2, a^2\Lambda^2_{\mathrm{QCD}}) + c_{a2p4}a^2\frac{p^{[4]}}{p^2} \\ &\qquad + c_{a4p4}a^4p^{[4]}. \end{aligned} \tag{3.17}$$

This fit gives $2w + 3$ parameters which are $Z_q^{\mathrm{hyp_{corrected}}}(a^2p^2, a^2\Lambda^2_{\mathrm{QCD}})$ for all a^2p^2 in the window, i.e., in the range $[a^2p^2_{\mathrm{min_{in}}}, a^2p^2_{\mathrm{max_{in}}}]$ (or, if the range size is even, one value is eliminated), and the parameters c_{a2p4} and c_{a4p4}.

D. Other lattice artefacts

There are ultraviolet artefacts which are functions of a^2p^2 and are thus insensitive to hypercubic biases and not corrected by the above-mentioned method. They will be corrected simply by assuming a term linear in a^2p^2 in the final fit and checking that the coefficient scales correctly for different lattice spacings. Then, after curing the hypercubic artefacts and removing such a linear term in a^2p^2, we will assume to be left with nonperturbative estimates of Z_q free of ultraviolet lattice artefacts and apply the same continuum formula (see Sec. V) for the results obtained from the three lattice data sets with different β. Of course, the results have to be converted from lattice to physical units with the appropriate lattice spacings before fitting with the continuum formula. Thus, if any noncured ultraviolet lattice artefacts still remain, they should emerge as a residual dependence of the fitting parameters on the lattice spacing that will be tested for our three lattice data sets.

To take into account the space-time anisotropy, which is a finite volume artefact, we can check the dependence of Z_q on a anisotropic quantity such as $p_4^2 - \vec{p}^2/3$. We did not see any sizeable effect of this parameter.

Finite volume artefacts are also studied as usual by a comparison of runs at different volume. We expect a small effect at large momenta, and our checks confirmed it, as well as the analysis of [7]. We will not consider this artefact anymore.

IV. LATTICE RESULTS AND HYPERCUBIC CORRECTIONS

The hypercubic artefacts generate on the raw lattice data, Z_q^{latt}, the so-called half-fishbone structure [12] shown in Fig. 1. In this figure, all the points labeled as explained in Eqs. (3.10) and (3.11) are plotted. The color code shows the value of the ratio $p^{[4]}/(p^2)^2$, which is between 0.25 and 1. The values closer to 1 are the ''less democratic'' or ''tyrannic'' ones. We see, as expected, that the tyrannic points are more affected by the artefacts. We also see that the gap between $Z_q^{\mathrm{latt}}(a^2p^2, a^4p^{[4]}, a^6p^{[6]}, ap_4, a^2\Lambda^2_{\mathrm{QCD}})$ at a given p^2 can be as large as 0.07, i.e, about 10%. Taking a naïve average without a correct treatment of this artefact would leave a systematic upward shift of about 5%. In Sec. III C we developed a nonperturbative method to cure this artefact (this method being split in two options, the SWF and the OWF). There also exist two other methods. The oldest one is the ''democratic selection.'' It amounts to keeping only, say, the points with ratio ≤ 0.3 in Fig. 1. One sees that it eliminates a lot of data, and it is still far from the egalitarian result (the lowest curve in Fig. 1) which we consider as better. We will thus not consider this democratic selection further. The second additional method for correcting hypercubic artefacts, which uses perturbative calculation, is detailed in the next section.

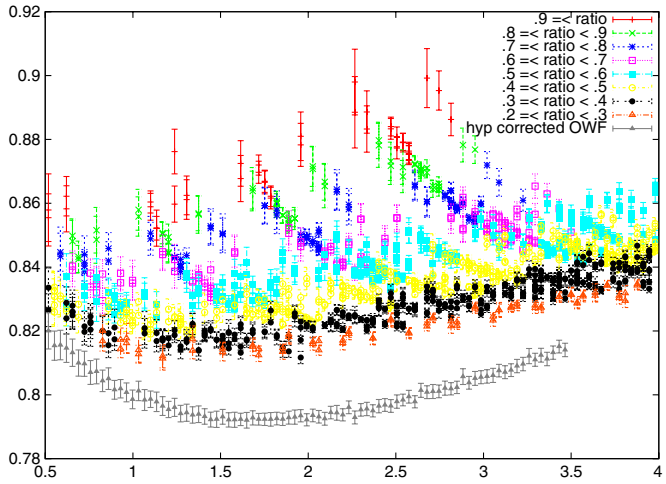

FIG. 1 (color online). This plot shows the raw data for $\beta = 3.9$, $Z_q^{\rm latt}(a^2p^2, a^4p^{[4]}, a^6p^{[6]}, ap_4, a^2\Lambda^2_{\rm QCD})$ in Eq. (3.15), in terms of a^2p^2 in the horizontal axis. The "half-fishbone" structure due to hypercubic artefacts is clearly seen. There is one point for every cubic (three-dimensional) orbit. The data-point [and color] code classifies the data according to their degree of "democracy" measured by the ratio $= p^{[4]}/(p^2)^2$. The lowest plot corresponds to the nonperturbatively hypercubic corrected data (or "egalitarian result") resulting from the one-window fit $Z_q^{\rm hyp_{corrected}}(a^2p^2, a^2\Lambda^2_{\rm QCD})$ in Eq. (3.17). The data correspond to $\beta = 3.9$, $a\mu = 0.004$, but the same features appear for all β's.

A. Perturbative correction

The perturbative method [26] consists of computing at one loop in lattice perturbation theory [27], and then, assuming that the lattice spacing artefacts are reliably described by the $O(g^2a^2)$ terms thus obtained, subtracting them from the lattice data. This method has been applied to quark bilinear operators in [28]. For comparison, we have applied this method here following the prescription described in Sec. 3.2.2 of [28] and also a variant of it.

Equation 24 in [26] may be written in Landau gauge as

$$Z_q^{\rm pert}(a^2p^2) = Z_q^{\rm tree}(a^2p^2) + \tilde{g}^2(b_{q1} + c_{q1}a^2p^2 + c_{q2}a^2p^2\log(a^2p^2) + c_{q3}\frac{a^2p^{[4]}}{p^2} + c_{q4}\frac{a^2p^{[4]}}{p^2}\log(a^2p^2)), \quad (4.1)$$

where, to follow [28], $\tilde{g}^2 = g^2_{\rm boosted}/(12\pi^2)$, with $g^2_{\rm boosted} = g^2_{\rm bare}/\langle{\rm plaquette}\rangle$. The coefficients are defined using the notations of Eq. (24) in [26]:

$$c_{q1} = \epsilon^{(2,4)}, \qquad c_{q2} = \frac{59}{240} + \frac{c_1}{2} + \frac{C_2}{60},$$
$$c_{q3} = \epsilon^{(2,1)} - \frac{3}{80} - \frac{C_2}{10}, \qquad c_{q4} = \frac{101}{120} - \frac{11}{30}C_2.$$

1. Prescription with $\tilde{p}_\mu$

Using the prescription of Eq. (35) in [28], for every cubic orbit we define the subtracted quantity as

$$Z_q^{\rm pert_{tilde}}(a^2p^2, a^4p^{[4]}, a^6p^{[6]}, ap_4, a^2\Lambda^2_{\rm QCD}) = Z_q^{\rm latt}(a^2p^2, a^4p^{[4]}, a^6p^{[6]}, ap_4, a^2\Lambda^2_{\rm QCD}) - \tilde{g}^2(c_{q1}a^2\tilde{p}^2 + c_{q2}a^2\tilde{p}^2\log(a^2\tilde{p}^2) + c_{q3}\frac{a^2\tilde{p}^{[4]}}{\tilde{p}^2} + c_{q4}\frac{a^2\tilde{p}^{[4]}}{\tilde{p}^2}\log(a^2\tilde{p}^2)). \quad (4.2)$$

The result of this subtraction is plotted in the left-hand side (lhs) of Fig. 2. The half-fishbone structure is still clearly visible for $a^2p^2 > 1.6$. We then try another prescription.

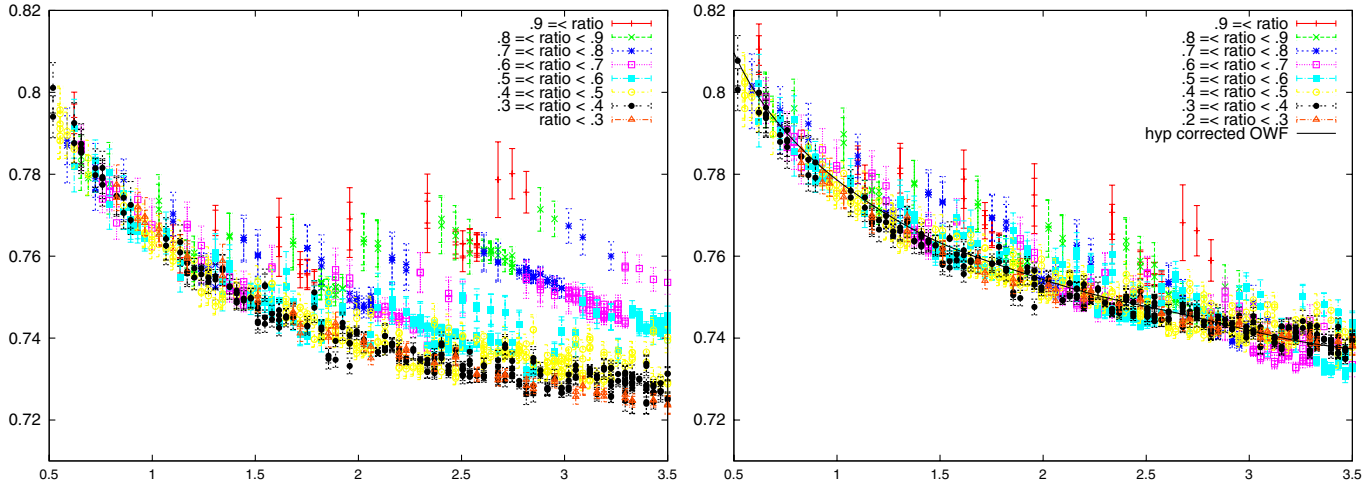

FIG. 2 (color online). Left-hand side: Data of Fig. 1 corrected by the perturbative subtraction formula of Eq. (4.2), Sec. IV A 1. Right-hand side: Same exercise with the prescription Eq. (4.3) with Eq. (4.1). The data-point [and color] code is the same as in Fig. 2, as is the ratio $= p^{[4]}/(p^2)^2$. The horizontal axis is a^2p^2 for both sides.

2. Prescription with p_μ

The trace of Eq. (3.9), which introduces $\tilde{p}_\mu$, had to be applied in Eq. (24) of [26] to obtain Eq. (4.1). We will now expand in p_μ before performing the trace and then keep the $O(g^2a^2)$ terms for subtraction. This gives, using again,

$$\begin{aligned} Z_q^{\mathrm{pert_{notilde}}}(a^2p^2, a^4p^{[4]}, a^6p^{[6]}, ap_4, a^2\Lambda_{\mathrm{QCD}}^2) \\ = Z_q^{\mathrm{latt}}(a^2p^2, a^4p^{[4]}, a^6p^{[6]}, ap_4, a^2\Lambda_{\mathrm{QCD}}^2) \\ - \tilde{g}^2\Big(c_{q1}a^2p^2 + c_{q2}a^2p\log(a^2p^2) \\ + c'_{q3}\frac{a^2p^{[4]}}{p^2} + c_{q4}\frac{a^2p^{[4]}}{p^2}\log(a^2p^2)\Big), \end{aligned} \tag{4.3}$$

where

$$c'_{q3} = \frac{\epsilon^{(0,1)}}{6} + \epsilon^{(2,1)} - \frac{3}{80} - \frac{C_2}{10} = c_{q3} + \frac{\epsilon^{(0,1)}}{6}. \tag{4.4}$$

This result is plotted in the rhs of Fig. 2. With this variant, the half-fishbone is significantly reduced, but a linear behavior on a^2p^2, not compatible with the logarithmic behavior predicted by perturbation theory, appears to emerge for the domain of larger a^2p^2. (This is clearly visible in the right plot of Fig. 2 for $a^2p^2 \gtrsim 2$–2.5.) This should be interpreted as an overcorrection for the dominant $O(4)$ artefact. The same is not manifest (not so clearly, at least) when applying the first prescription for the perturbative hypercubic correction, as can be concluded after comparing left and right plots in Fig. 2.

3. Lessons about the perturbative method

We see that the two prescriptions start differing significantly at $a^2p^2 \simeq 1$, which is not surprising since higher-order terms become significant; for example, an $a^4p^{[4]}$ is also of order 1 for tyrannic points, while $a^2p^2 - a^2\tilde{p}^2 \simeq 0.3$. The perturbative method goes in the right direction, but it is impossible to know *a priori* its quality without performing the tests we propose here. The method contains several ambiguities: What to take for the coupling constant? Use p_μ or $\tilde{p}_\mu$? Contrary to the nonperturbative method, this method provides both the hypercubic corrections and the $O(a^2p^2)$ ones. Conceptually, the perturbative method is very useful as it exhibits qualitative aspects which may guide the use of the nonperturbative one; for example, it justifies the smoothness of the variation of the derivative R, Eq. (3.15), as a function of a^2p^2 as well as that of the slope in a^2p^2. Finally, we shall see that it gives results similar to the nonperturbative ones.

B. Nonperturbative hypercubic correction

We now apply the nonperturbative correction. First of all, we check that the lattice estimates of Z_q for any fixed value of a^2p^2, within our momentum range, show a regular behavior as a function of the only $H(4)$-invariant, $p^{[4]}$, that we will expand in: a linear fit gives proper account of our estimates for any $a^2p^2 \lesssim 3.5$. This can be seen in the plots in Fig. 3, obtained for some representative values of a^2p^2. Thus, we only expand in $p^{[4]}$ since the higher-order terms

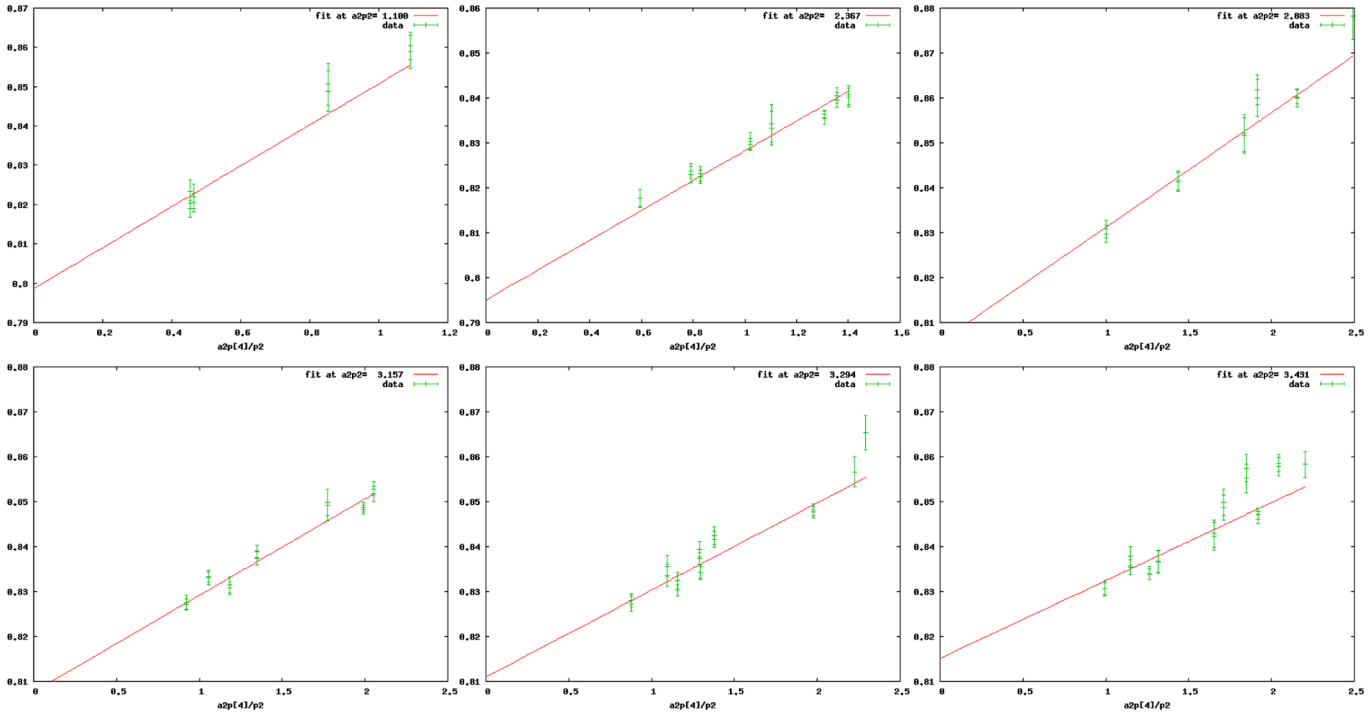

FIG. 3 (color online). We show the lattice estimates of Z_q in terms of $a^2p^{[4]}/p^2$ for some representative values of the fixed lattice momentum, $a^2p^2 = 1.100, 2.367, 2.883, 3.15\,7, 3.294, 3.431$. Only for the last one, corresponding to the maximum lattice momentum we used for our analysis, some small deviation from the linear behavior seems to appear at large values of $a^2p^{[4]}/p^2$.

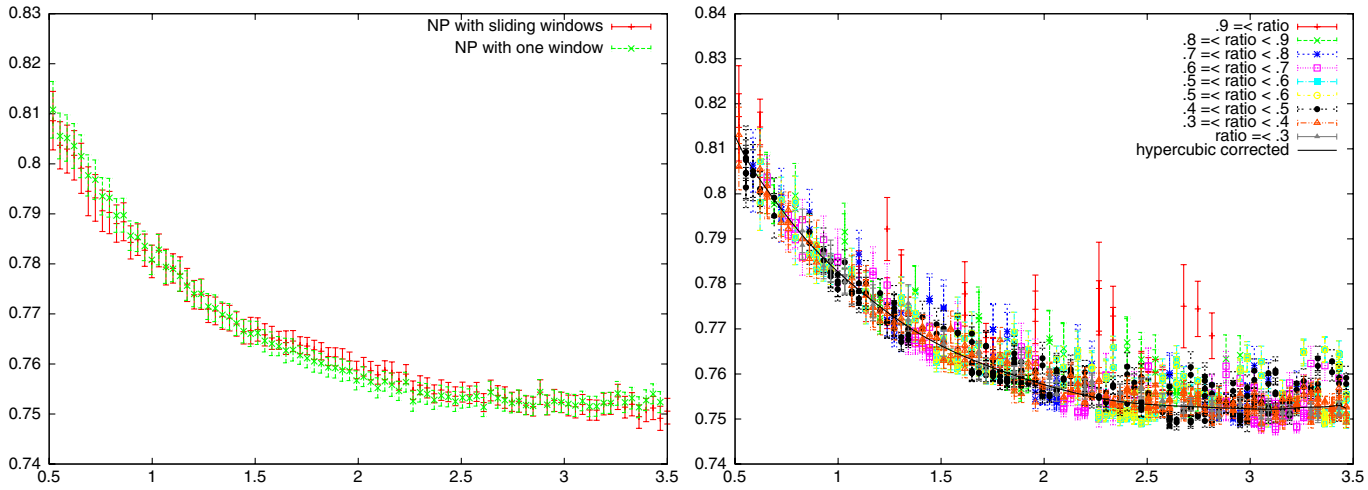

FIG. 4 (color online). On the left-hand side, we compare, for $\beta = 3.9$, $a\mu = 0.004$, the nonperturbatively corrected Z_q from the sliding-windows fit (SWF), Sec. III C 1 and from the one-window fit (OWF), Sec. III C 2. To better show the running, we have also subtracted the $O(a^2p^2)$ artefact, which will be computed below. On the right-hand side, we show, using the OWF, the nonperturbatively subtracted data Eq. (4.5). There is one point for every cubic (three-dimensional) orbit. The data-point [and color] code and the definition of the parameter ratio are the same as in Fig. 2. The black line corresponds to the OWF's nonperturbatively corrected result: $Z_q^{\mathrm{hyp}_{\mathrm{corrected}}}(a^2p^2, a^2\Lambda^2_{\mathrm{QCD}})\chi$ of Eq. (3.17). The $O(a^2p^2)$ has also been subtracted. The horizontal axis is a^2p^2.

turn out to be negligible in our momentum range. We also check that introducing a cutoff, $a^2p^{[4]}/p^2 \lesssim 1.5$–$2.0$, for the data to be used in the linear extrapolation does not modify our extrapolated results for Z_q at any a^2p^2, apart from statistical fluctuations. This is also clear from Fig. 3, where only for the largest lattice momentum, $a^2p^2 = 3.431$, does there appear to be some small deviation from the linear behavior above $a^2p^{[4]}/p^2 = 2.0$. Even for this case, the slope computed through the OW fit appears not to be essentially affected by these deviated data.

1. Sliding-windows fit versus one-window fit

In Sec. III C we presented two types of fits, similar in spirit: the sliding-windows fit (SWF) described in Sec. III C 1, which amounts to using Eq. (3.14) combined with Eq. (3.15), and the one-window fit (OWF) described in Sec. III C 2, which amounts to using Eq. (3.16). In the lhs of Fig. 4 we show, in the case of $\beta = 3.9$, the comparison of hypercubic corrected data after applying OWF and SWF. The difference does not appear to be large, which is rather encouraging. The OWF gives a slightly smoother result. For this value of β, the chi-squared is not good (see Table II), but remember that it uses only two hypercubic parameters. Chi-squared for the other β's are better.

2. Half-fishbone reduction test

We need also to apply the half-fishbone reduction test as in the perturbative case, i.e., to subtract the hypercubic correction to the raw data of every cubic orbit. We present the OWF result. From Eq. (3.17), the subtraction amounts to

$$Z_q^{\mathrm{nonpert}_{\mathrm{OWF}}}(a^2p^2, a^4p^{[4]}, a^6p^{[6]}, ap_4, a^2\Lambda^2_{\mathrm{QCD}}) = Z_q^{\mathrm{latt}}(a^2p^2, a^4p^{[4]}, a^6p^{[6]}, ap_4, a^2\Lambda^2_{\mathrm{QCD}}) - c_{a2p4}a^2\frac{p^{[4]}}{p^2} - c_{a4p4}a^4p^{[4]}. \quad (4.5)$$

The result is shown in the rhs of Fig. 4, one point per cubic orbit. The nonperturbatively corrected $Z_q^{\mathrm{hyp}_{\mathrm{corrected}}}(a^2p^2, a^2\Lambda^2_{\mathrm{QCD}})$ of Eq. (3.17) is represented by the black line in the rhs of Fig. 4. It is well in the middle of the subtracted points, as we would expect.

It is seen that the half-fishbones have been strongly reduced. One sees a remainder of these artefacts due to the less democratic, or tyrannic points. These have only one nonvanishing component or one large and a very small one. These points are not so many as seen in the plot; their orbits are small, which explains the larger error bars. We

TABLE II. Results for the slope in $a^2p^{[4]}/p^2$ and $a^4p^{[4]}$ and the same divided by g^2 in the one-window fit.

β	a^2 fm^2	c_{a2p4}	c_{a4p4}	c_{a2p4}/g^2	c_{a4p4}/g^2	χ^2/d.o.f
3.9	0.00689	0.067(4)	−0.0149(10)	0.044(3)	−0.0097(7)	4.1
4.05	0.00456	0.065(3)	−0.0144(5)	0.044(2)	−0.0097(3)	0.53
4.2	0.00303	0.055(11)	−0.0124(4)	0.039(8)	−0.0089(3)	0.98

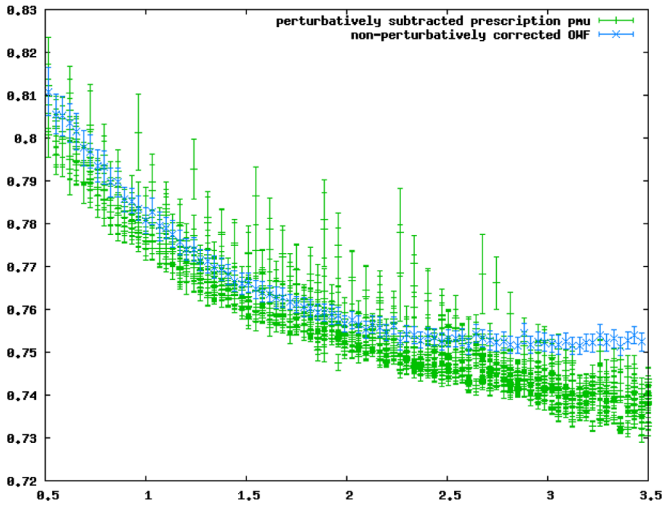

FIG. 5 (color online). We plot together, for comparison, $\beta = 3.9$, the perturbatively subtracted results defined in Sec. IV A 2, i.e., all the points of the right-hand side of Fig. 2 [here in green], and the nonperturbatively corrected ones with OWF, i.e., the line-with-X [green] points of the left-hand side of Fig. 4 [this time in blue].

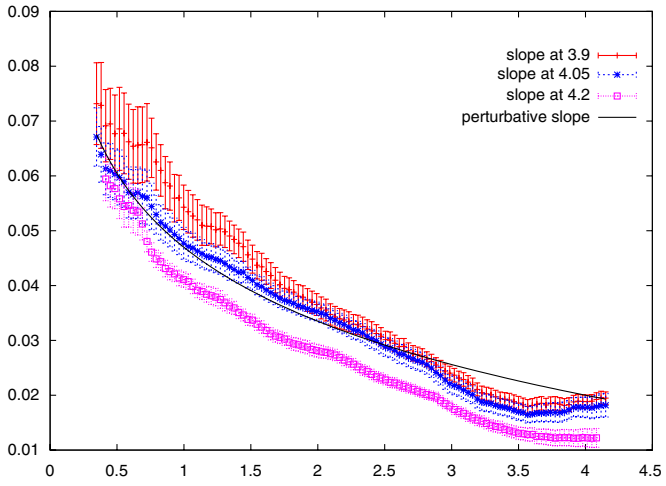

FIG. 6 (color online). The three lattice slopes R defined in Eq. (3.15) for the three lattice spacings and the perturbative one $R_{\rm pert} = c'_{q3} + c_{q4}\log(a^2p^2)$ for $\beta = 3.9$, in terms of a^2p^2 in the horizontal axis.

have checked that these tyrannic points have indeed a small impact on the hypercubic corrected result.

Finally, for the sake of comparison of results obtained after applying perturbative and nonperturbative hypercubic corrections, we plot together in Fig. 5 the perturbatively subtracted results defined in Sec. IV A 2 and the nonperturbatively corrected ones with OWF, at $\beta = 3.9$.

3. The slopes in $p^{[4]}$

The sliding-windows fit solves for every window a value for the slope $R(a^2p^2)$ [Eq. (3.15)], i.e., the derivative $\partial Z_q^{\rm latt}/\partial(a^2p^{[4]}/p^2)$. This allows for a study of the shape of this function R. In Fig. 6 we plot this slope R defined in Eq. (3.15) for the three values of β. We also plot the equivalent slope using the perturbative formula with the p_μ prescription for $\beta = 3.9$, Sec. IV A 2: $R_{\rm pert} = c'_{q3} + c_{q4}\log(a^2p^2)$, c'_{q3} defined in Eq. (4.4) and c_{q4} in Eq. (4.2). We see that this perturbative slope is in fair agreement with the nonperturbative one, explaining the good elimination of half-fishbones in the rhs in Fig. 2.

The three nonperturbative data in Fig. 6 give the impression to be affine (a constant minus a linear term) over a rather large momentum interval. This is what is expressed in Eq. (3.16) from where we have deduced the one-window fit: a fit over the full range (0.5–3.5) with only two hypercubic parameters.[4]

[4]Of course, there are additionally as many hypercubic insensitive parameters as there are values of p^2 in the range, which are simply the values of $Z_q^{\rm hyp_{corrected}}(a^2p^2, a^2\Lambda^2_{\rm QCD})$.

The fitted values for c_{a2p4} and c_{a4p4} from the one-window fit are given in Table II as well as the same divided by g^2, since perturbation theory expects at least for c_{a2p4} to be $\propto g^2$. Before dividing by g^2, a small scaling violation is apparent, which corresponds to the nonoverlap of the curves at different β's in Fig. 6. It appears on Table II that dividing by g^2 improves the scaling significantly. The χ^2 in Table II is not good for $\beta = 3.9$, apparently due to some structure at the lower end of the plot.

V. RUNNING INCLUDING $\langle A^2\rangle$ CORRECTIONS FROM OPE

In this section, we will check the running of Z_q. For this purpose, we shall use both the formula Eq. (A24) derived in the Appendix, to which we add a lattice artefact term $\propto a^2p^2$ not yet subtracted:

$$\begin{aligned} Z_q^{\rm hyp_{corrected}}(a^2p^2) &= Z_q^{\rm pert\,RI'}(\mu'^2)c^{\rm RI'}_{0Z_q}\left(\frac{p^2}{\mu'^2},\alpha(\mu')\right) \\ &\times\left(1+\frac{c^{\overline{\rm MS}}_{2Z_q}\left(\frac{p^2}{\mu^2},\alpha(\mu)\right)}{c^{\rm RI'}_{0Z_q}\left(\frac{p^2}{\mu^2},\alpha(\mu)\right)}\frac{c^{\rm W\overline{MS}}_{2Z_q}\left(\frac{p^2}{\mu^2},\alpha(\mu)\right)}{c^{\overline{\rm MS}}_{2Z_q}\left(\frac{p^2}{\mu^2},\alpha(\mu)\right)}\frac{\langle A^2\rangle_{\overline{\rm MS},\mu^2}}{32p^2}\right) \\ &+ c_{a2p2}a^2p^2, \end{aligned} \tag{5.1}$$

and a formula including only an OPE correction with a tree-level Wilson coefficient,

$$\begin{aligned} Z_q^{\rm hyp_{corrected}}(a^2p^2) &= Z_q^{\rm pertRI'}(\mu'^2)c^{\rm RI'}_{0Z_q}\left(\frac{p^2}{\mu'^2},\alpha(\mu')\right) \\ &\times\left(1+\frac{c_{1/p2}}{p^2}\right)+c_{a2p2}a^2p^2, \end{aligned} \tag{5.2}$$

where $c_{1/p2} = g^2\langle A^2\rangle/12$. We use $\mu' = \mu = 10$ GeV as the renormalization scale; $c^{\mathrm{RI}'}_{0Z_q}(p^2, \mu^2)$ is computed from the four-loop perturbative running of Z_q [13],

$$c^{\mathrm{RI}'}_{0Z_q}(p^2, \mu^2) \equiv \frac{Z_q^{\mathrm{pert\ RI}'}(p^2, g^2_{\mathrm{bare}})}{Z_q^{\mathrm{pert\ RI}'}(\mu^2, g^2_{\mathrm{bare}})}; \tag{5.3}$$

$c^{\overline{\mathrm{MS}}}_{2Z_q}(p^2, \mu^2)$ is the three-loop Wilson coefficient of $\langle A^2\rangle$ in the expansion of Z_q [9]; and the ratio

$$\frac{c^{\mathrm{W}\overline{\mathrm{MS}}}_{2Z_q}\left(\frac{p^2}{\mu^2}, \alpha(\mu)\right)}{c^{\overline{\mathrm{MS}}}_{2Z_q}\left(\frac{p^2}{\mu^2}, \alpha(\mu)\right)} = \frac{1 - 0.1317\alpha^2(\mu) - 0.5155\alpha^3(\mu)}{1 - 0.1317\alpha^2(p) - 0.5155\alpha^3(p)} \tag{5.4}$$

is obtained in the Appendix. We express the lattice spacing (cutoff) dependence as a dependence in g^2_{bare}. $Z_q^{\mathrm{pert\ RI}'}(\mu^2, g^2_{\mathrm{bare}})$ is the perturbative contribution to Z_q at the scale μ in the RI'-MOM scheme. In other words,

$$\begin{aligned} Z_q^{\mathrm{RI}'}(p^2, g^2_{\mathrm{bare}}) &= Z_q^{\mathrm{pert}RI'}(p^2, g^2_{\mathrm{bare}}) \\ &\times \left(1 + \frac{c^{\overline{\mathrm{MS}}}_{2Z_q}\left(\frac{p^2}{\mu^2}, \alpha(\mu)\right)}{c^{\mathrm{RI}'}_{0Z_q}\left(\frac{p^2}{\mu^2}, \alpha(\mu)\right)} \frac{c^{\mathrm{W}\overline{\mathrm{MS}}}_{2Z_q}\left(\frac{p^2}{\mu^2}, \alpha(\mu)\right)}{c^{\overline{\mathrm{MS}}}_{2Z_q}\left(\frac{p^2}{\mu^2}, \alpha(\mu)\right)} \frac{\langle A^2\rangle_{\overline{\mathrm{MS}}, \mu^2}}{32p^2}\right). \end{aligned} \tag{5.5}$$

From now on, Z_q^{pert} will refer to $Z_q^{\mathrm{pert}RI'}$. We fit three parameters: Z_q^{pert}, c_{a2p2} and alternatively $c_{1\mathrm{over}p2}$ (which amounts to a tree-level treatment of the c_{2Z_q} coefficient) or the vacuum expectation value (VEV) $g^2\langle A^2\rangle$. In order to estimate the systematic errors, we will treat in parallel the one-window fit and the sliding-windows one. The results are reported in Tables III and IV and Figs. 7 and 8. The coefficient c_{a2p2} obviously refers to an $O(4)$ invariant lattice-spacing artefact which is not detected by our non-perturbative hypercubic correction method. We see in the right plot of Fig. 7 as well as in the tables that this coefficient scales very well when expressed in lattice units, as it should be. The coefficient of $1/p^2$, if it is related to a VEV $\langle A^2\rangle$, should rather scale in physical units. We see in the left plot of Fig. 7 that a constant value is rather well verified although with large errors. The results presented in Tables III and IV show that the estimates for $g^2\langle A^2\rangle$ from OPE expressions with Wilson coefficient from the Chetyrkin-Maier (CM) three-loop expression are systematically about 20% below the ones from the tree-level one.

TABLE III. Results for $Z_q^{\mathrm{pert}}(10\ \mathrm{GeV})$ and c_{a2p2} Eq. (5.1) from the one-window fit and the estimated $g^2\langle A^2\rangle$ VEV from the $1/p^2$ term and from the Chetyrkin-Maier [9] (CM) Wilson coefficient. Notice that Z_q^{pert} and c_{a2p2} from these two fits are very close.

β	a^2 fm^2	Z_q^{pert}	c_{a2p2}	$g^2\langle A^2\rangle_{\mathrm{tree}}$	$g^2\langle A^2\rangle_{CM}$
3.9	0.00689	0.726(5)	0.0201(13)	3.20(38)	2.62(31)
4.05	0.00456	0.742(5)	0.0200(15)	3.09(65)	2.57(54)
4.2	0.00303	0.760(3)	0.0194(8)	3.23(55)	2.74(47)
Average			0.0197(6)	3.18(28)	2.64(23)

A. Residual lattice artefacts

Equation (5.1) to be applied for the fits of our three lattice data sets, after the hypercubic lattice artefacts have been properly cured, describes the running of Z_q by a continuum formula and removes any nonhypercubic lattice artefacts by a linear term in a^2p^2. Thus, we are initially left with three free parameters: $g^2\langle A^2\rangle$ and $\Lambda_{\overline{\mathrm{MS}}}$ from the continuum formula and c_{a2p2} from the linear term. To fit the lattice data, everything is converted to physical units by applying the lattice spacings given in Table I and taken from Ref. [7], and we also borrow the estimate provided by the same paper to fix the value of $\Lambda_{\overline{\mathrm{MS}}}$. Then, as long as hypercubic and nonhypercubic lattice artefacts are properly removed, the same continuum formula has to work for the three lattices, and the three fitted values of $g^2\langle A^2\rangle$ are expected to be compatible. The same should happen for the three fitted values of c_{a2p2}. In other words, as we previously emphasized, a final check of the procedure we followed to cure ultraviolet lattice artefacts will result from studying the impact of the residual dependence, if any, on the lattice spacing for $g^2\langle A^2\rangle$ and c_{a2p2}. This is done in Fig. 9, where we extrapolate to zero lattice spacing through a linear fit of the three estimates for both parameters in Tables III and IV with OW and SW fits. The results of the extrapolations appear in

TABLE IV. The same calculations as in Table III using the data from the sliding-windows fit to hypercubic corrections.

β	a^2 fm^2	Z_q^{pert}	c_{a2p2}	$g^2\langle A^2\rangle_{\mathrm{tree}}$	$g^2\langle A^2\rangle_{CM}$
3.9	0.00689	0.741(3)	0.0161(9)	2.07(37)	1.70(31)
4.05	0.00456	0.753(5)	0.0168(14)	2.13(52)	1.78(43)
4.2	0.00303	0.771(3)	0.0164(9)	1.59(60)	1.36(51)
Average			0.0165(6)	1.99(26)(27)	1.65(22)(27)

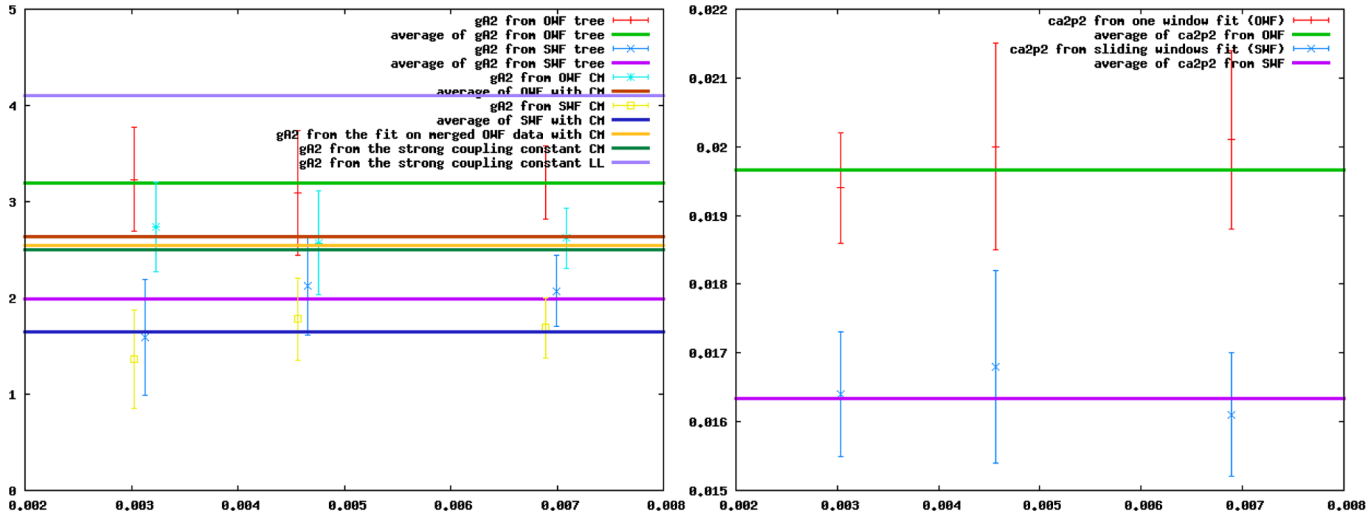

FIG. 7 (color online). We plot the values of the fitted slopes c_{a2p2} (on the right-hand side) and the condensate $g^2\langle A^2\rangle$ (on the left) as extracted from the $1/p^2$ contribution to the fit; see Tables III, IV, and VIII. In the left plot, we show the results from the OWF and from the SWF. It can be seen that the $O(\alpha^4)$ formula for the Wilson coefficient computed by Chetyrkin and Maier [9] of $\langle A^2\rangle$ (indicated by the "CM" initials) is about 20% below the tree level result. We show the value obtained from the merged results of the three lattice spacings, Table VIII. Finally, for the sake of comparison we show the result from the strong coupling constant of [7]. The horizontal axis is a^2 in fm^2.

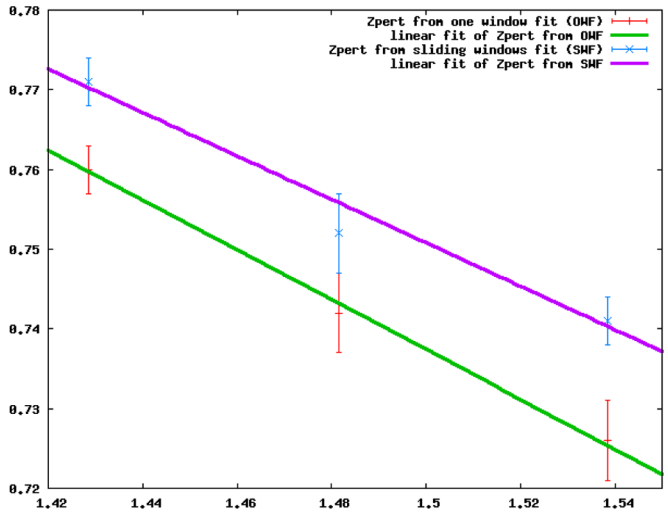

FIG. 8 (color online). We show the value of $Z_q^{\rm pert}$ defined in Eq. (5.1) for all three lattice spacings as a function of the bare coupling constant $g^2 = 6/\beta$. The points with X were obtained through the SWF procedures and fitted linearly (upper solid line); the lower points and lower solid line correspond to the OWF procedure.

Table V compared to the averaged values: they are compatible within the range of statistical errors.[5]

We can thus conclude that no sizeable ultraviolet artefact remains after applying our H(4)-extrapolation and removing the linear term in a^2p^2. The same conclusion can be obtained by invoking the merged analysis in Sec. V E, and notice in Fig. 11 that, after converting to physical units and rescaling with the ratios of $Z_q^{\rm pert}$ given in Table III, the data from the three lattices corrected for all lattice artefacts match pretty well. This scaling in physical units can be also taken as a good indication for the negligible impact of finite-volume artefacts within our momentum range.

B. Analysis from the nonperturbative hypercubic corrections

1. Comparison of the running from the OWF and the SWF

From Tables III and IV, we see that $g^2\langle A^2\rangle$ is systematically larger for the OWF than for the SWF. At first sight, that seems surprising since the OWF and SWF hypercubic corrected data are very similar (see Fig. 4). One reason is the correlation between c_{a2p2} and $g^2\langle A^2\rangle$: c_{a2p2} is also systematically larger for the OWF than for the SWF. This correlation is understandable as the a^2p^2 increases with p^2 while $1/p^2$ decreases. This is compensated by a $Z_q^{\rm pert}$ smaller for the OWF than for the SWF. We will consider these differences as a systematic uncertainty in our fits and count them in the errors.

2. Dependence on the fitting range

An additional test is to look for the effect of the fitting range. The results are shown in Table VI and Fig. 10. One sees again a correlation between the c_{a2p2} slope and $g^2\langle A^2\rangle$. Both decrease when the fitting range shortens while

[5]Furthermore, we underestimate the statistical error for the extrapolated value because it is computed by applying the optimal slope without errors.

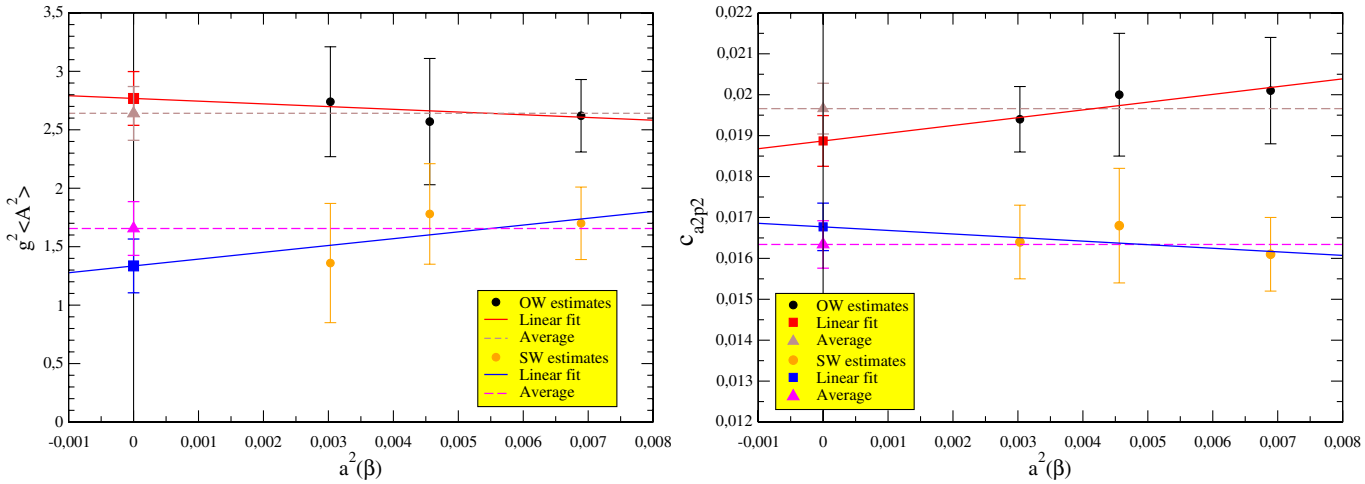

FIG. 9 (color online). Linear extrapolation to zero lattice spacing for $g^2\langle A^2\rangle$ (left) and c_{a2p2} (right) obtained by OW (black circles) and SW (paler [orange] circles) fits. The dotted lines correspond to the averaged values from OW (upper [brown]) and SW (lower [magenta]) fits.

correlatively Z_q^{pert} increases. The lhs of Fig. 10 explains how this happens: when the range is shorter, the error bars allow for a less curved fit. But the fit never reaches a value such that $g^2\langle A^2\rangle$ disappears. The shortest window $0.5 < a^2p^2 < 2.0$ gives the smallest value for $g^2\langle A^2\rangle$ but still 4 sigmas away from 0.

C. Analysis from the perturbative hypercubic corrections

It is then useful to check if similar results are obtained after a perturbative correction to the hypercubic artefacts has been applied.

We have used two prescriptions to apply the perturbative corrections. With the data obtained from the $\tilde{p}_\mu$ prescription, Sec. IV A 1, we perform an average on all the cubic orbits of every p^2 after a democratic selection $p^{[4]}/(p^2)^2 < 0.3$. This leaves us with not too many points, and it results in rather large statistical errors. We then perform the same running fit on the nonperturbatively hypercubic corrected results: we fit with one perturbative running contribution, one $1/p^2$ contribution, and one $\propto a^2p^2$ artefact. With the data from the p_μ prescription, Sec. IV A 2, we perform the same fit over an average on all the cubic orbits of every p^2 without any democratic selection, since the hypercubic artefacts have already been efficiently reduced. The results are shown in Table VII.

TABLE V. Results from the linear extrapolation and averages of the values of $g^2\langle A^2\rangle$ obtained by the OW and SW fits.

		$g^2\langle A^2\rangle(\text{GeV}^2)$	c_{a2p2}
OW	Linear fit	2.77(23)	0.0189(6)
	Average	2.64(23)	0.0197(6)
SW	Linear fit	1.34(22)	0.0167(6)
	Average	1.65(22)	0.0165(6)

A first remark is that the c_{a2p2} coefficients are compatible with zero, indicating that the perturbative correction has efficiently eliminated this artefact. The coefficient of the $1/p^2$ nonperturbative contribution is found to be different from zero, in the same ballpark as the results from the nonperturbative hypercubic correction, in Tables III and IV. The $\tilde{p}_\mu$ prescription has too-large errors to be conclusive but the p_μ is five sigmas away from zero, very similar to the results in Table IV. The value of Z_q^{pert} for the $\tilde{p}_\mu$ prescription is rather low but compatible within less than two sigmas from the result for $\beta = 3.9$ in Table IV.

D. Running of Z_q^{pert}

It is interesting to consider the dependence of Z_q^{pert} as a function of g^2. This is plotted in Fig. 8 both for the OWF and the SWF. It is strikingly linear, especially for the OWF. Indeed, from Eq. (24) of [26] perturbation theory gives a linear dependence with a slope $\simeq -0.19$. This comes from the coefficient b_{q1} in Eq. (4.1) which is multiplied by g^2. In our case, we find from the OWF

TABLE VI. For $\beta = 3.9$, results for the Z_q^{pert} ($\mu = 10$ GeV) and c_{a2p2} Eq. (5.1) from the one-window hypercubic corrected data and the estimated $g^2\langle A^2\rangle$ VEV from the $1/p^2$, plotted as a function of the upper bound of the fitting range (in GeV).

Upper bound	Z_q^{pert}	c_{a2p2}	$g^2\langle A^2\rangle_{tree}$	$g^2\langle A^2\rangle_{CM}$
2.0	0.754(6)	0.0089(21)	1.58(39)	1.28(32)
2.5	0.745(6)	0.0130(18)	2.05(37)	1.67(30)
3.0	0.733(5)	0.0175(15)	2.73(36)	2.22(30)
3.5	0.726(5)	0.0201(13)	3.20(38)	2.62(31)

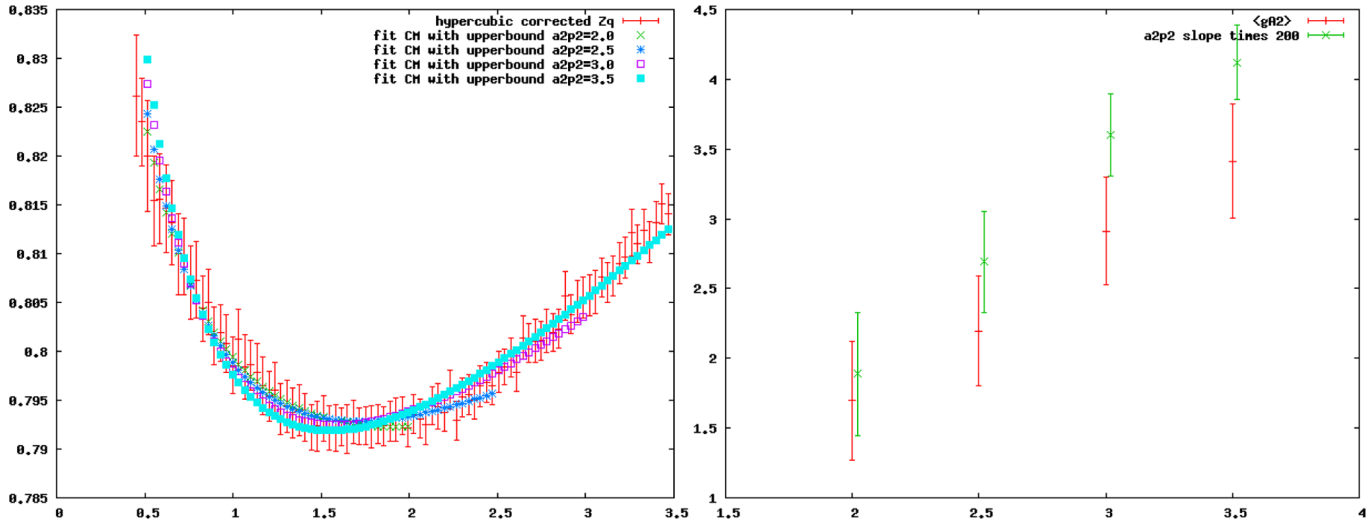

FIG. 10 (color online). In the right-hand plot we show how $g^2\langle A^2\rangle$, fitted with the CM Wilson coefficient, depends on the upper range of our fits, always starting at $a^2p^2 = 0.5$ for $\beta = 3.9$. The points correspond to $a^2p^2 < 2.0, 2.5, 3.0, 3.5$. The right-hand side plot also shows the a^2p^2 artefact slope. We find again a positive correlation between both series of data. The left-hand side of the plot illustrates this, showing for the same data how the fitting function depends on the upper bound of the range.

$$Z_q^{\text{pert}}((10\,\text{GeV})^2, g^2_{\text{bare}}) = 0.737(3) - 0.313(6)(g^2_{\text{bare}} - 1.5),$$
$$Z_q^{\text{pert}}((2\,\text{GeV})^2, g^2_{\text{bare}}) = 0.766(3) - 0.324(6)(g^2_{\text{bare}} - 1.5); \tag{5.6}$$

and from the SWF

$$Z_q^{\text{pert}}((10\ \text{GeV})^2, g^2_{\text{bare}}) = 0.751(2)(7) - 0.273(6)(^{0.002}_{-0.038}) \times (g^2_{\text{bare}} - 1.5),$$
$$Z_q^{\text{pert}}((2\ \text{GeV})^2, g^2_{\text{bare}}) = 0.780(3)(7) - 0.284(6)(^{0.002}_{-0.040}) \times (g^2_{\text{bare}} - 1.5). \tag{5.7}$$

We see that the coefficients of g^2,

$$\frac{\partial Z_q^{\text{pert}}((2\text{GeV})^2, g^2_{\text{bare}})}{\partial g^2} = \begin{cases} -0.324(6) & \text{OWF} \\ -0.284(6) & \text{SWF} \end{cases}, \tag{5.8}$$

are significantly larger than the perturbatively expected -0.19. But the linear behavior predicted by perturbation theory is well verified, especially for OWF.

TABLE VII. For $\beta = 3.9$, results for the $Z_q^{\text{pert}}(\mu^2, g^2_{\text{bare}})$ ($\mu =$ 10 GeV) and c_{a2p2} Eq. (5.1) and $g^2\langle A^2\rangle$ from the lattice data after a perturbative hypercubic correction. $g^2\langle A^2\rangle$ is estimated at tree level (fourth column) and at the order $\mathcal{O}(\alpha^4)$ (fifth column) from the $1/p^2$ contribution.

Prescription	Z_q^{pert}	c_{a2p2}	$g^2\langle A^2\rangle_{tree}$	$g^2\langle A^2\rangle_{CM}$
$\tilde{p}_\mu$	0.712(11)	−0.0026(23)	2.98(1.49)	2.53(1.23)
p_μ	0.745(3)	−0.0061(8)	1.76(35)	1.45(29)

E. Merging the three lattice spacings

From Eqs. (5.1) and (5.5) it is clear that

$$Z_q^{\text{RI}'}(p^2, g^2_{\text{bare}}) = Z_q^{\text{hyp}_{\text{corrected}}}(a^2p^2) - c_{a2p2}a^2p^2. \tag{5.9}$$

In this section, we use the one-window fit, Sec. III C 2, and the momentum p^2 is now expressed in physical units. For the coefficient c_{a2p2}, we use the values in Table III. The three $Z_q^{\text{RI}'}$ for the three β's do not match due to the running of Z_q as a function of the lattice spacing. To make them match, it turns out that it is enough to take into account the ratios of Z_q^{pert}'s given in Table III. We plot on the lhs of Fig. 11 the three sets of data where the $\beta = 4.05, 4.2$ ones have been rescaled to the $\beta = 3.9$ scale. We see a rather good overlap. There is, however, a flattening at the right end of every β which stays within one sigma from the other β's. We understand it as a failure of the hypercubic artefacts treatment. On the rhs side of Fig. 11, we plot the same number corrected for perturbative running by the multiplicative factor $0.726/Z_q^{\text{pert}}(p^2, 6/3.9)$, where 0.726 is taken from Table VIII. The black line is just the nonperturbative contribution added to 0.726. The comparison of both plots in Fig. 11 is enlightening. We see that the nonperturbative term contributes about one-half of the change between the smallest momenta and the largest ones. Both the perturbative running and the nonperturbative contribution are convex, which makes it difficult to disentangle them. But we also see that the perturbative running cannot account for the full variation of the data. The best-fit parameters resulting from this merged analysis can be found in Table VIII, where we use $g^2_{\text{bare}} = 6.0/3.9$ since we have rescaled all the data to the $\beta = 3.9$ scale. The values in Table VIII for $g^2(\mu^2)\langle A^2\rangle_{\mu^2\text{merged}}$ turn out to

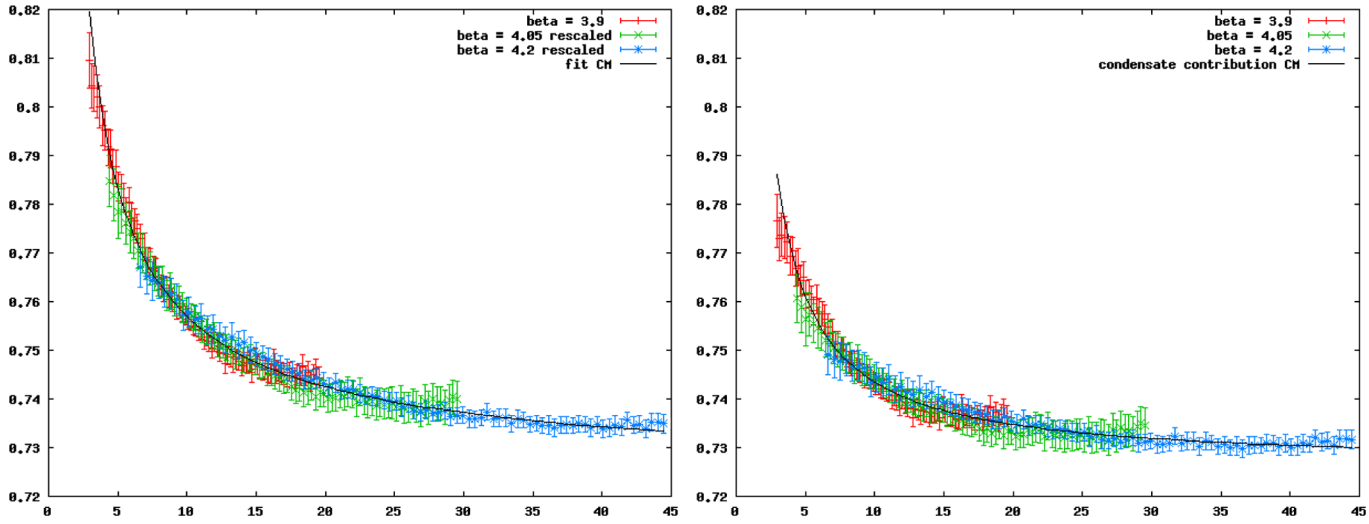

FIG. 11 (color online). The merged plot with the OWF results at $\beta = 4.05$ and $\beta = 4.2$, rescaled to the $\beta = 3.9$ thanks to the ratios of $Z_q^{\rm pert}$ given in Table III. The left-hand side shows the data corrected for all lattice artefacts. The right-hand side shows the same data further corrected by the perturbative running factor up to 10 GeV. The horizontal axis is p^2 in GeV^2. The black line on the left corresponds to the global fit with perturbative running and CM (three loops) Wilson coefficient for the $1/p^2$ term. The black line on the right corresponds only to the $1/p^2$ times the three loops Wilson coefficient added to $Z_q^{\rm pert}((10\ {\rm GeV})^2, 6/3.9) = 0.726$.

be rather central in the set of values of Tables III and IV. The value for $Z_q^{\rm pert}(10\ {\rm GeV}, 6./3.9)$ is in very good agreement with Eq. (5.6): $Z_q^{\rm pert}(10\ {\rm GeV}, 6./3.9) = 0.725(3)$.

F. Summarizing

Many of our results for $g^2\langle A^2\rangle$ are shown in the lhs of Fig. 7. We did not plot the range-dependent data to not overload the plot, but they fall in the range covered by the data plotted in Fig. 7. To summarize our results and estimate the systematic uncertainty, we consider the set of values in Tables III, IV, VI, and VIII. We will make a separate average for the tree-level data and the $O(\alpha^4)$ (CM) ones since the comparison with estimates from other quantities, such as the coupling constant, need to be performed in the same scheme, expansion, order, and scale. The scheme is $\overline{\rm MS}$, and the precise implementation is detailed in the Appendix. We computed an average of all above-listed data, weighted by their inverse-squared error. The inverse-squared statistical error is the sum of the inverse-squared errors. The systematic error is taken so as to incorporate the central values within the error bars. This is rather conservative. For $Z_q^{\rm pert}$, we average Eqs. (5.6) and (5.7) with a similar method. We get:

TABLE VIII. Merged data from three β's: Results for the $Z_q^{\rm pert}$ ($\mu = 10$ GeV) rescaled to $\beta = 3.9$, from the one-window hypercubic corrected data (OWF) with tree level and the three-loop formula, Eq. (A24).

$Z_q^{\rm pert}$	$g^2\langle A^2\rangle_{\rm tree}$	$g^2\langle A^2\rangle_{CM}$
0.726(2)	3.13(43)	2.55(36)

$$
\begin{aligned}
g^2(\mu^2)\langle A^2\rangle_{\mu^2{\rm tree}} &= 2.45(14)(^{+0.78}_{-0.87})\,{\rm GeV}^2 \quad \mu = 10\,{\rm GeV},\\
g^2(\mu^2)\langle A^2\rangle_{\mu^2 CM} &= 2.01(11)(^{+0.61}_{-0.73})\,{\rm GeV}^2\,\mu = 10\,{\rm GeV},\\
Z_q^{\rm pert}((10\,{\rm GeV})^2, g^2_{\rm bare}) &= 0.744(2)(7) - 0.311(6)(^{+0.002}_{-0.038})\\
&\quad \times (g^2_{\rm bare} - 1.5),\\
Z_q^{\rm pert}((2\,{\rm GeV})^2, g^2_{\rm bare}) &= 0.773(3)(7) - 0.323(6)(^{+0.002}_{-0.040})\\
&\quad \times (g^2_{\rm bare} - 1.5),
\end{aligned}
\tag{5.10}
$$

where the first error is statistical and the second is the systematic one. The values of $Z_q^{\rm RI'}(p^2, g^2_{\rm bare})$ may then be derived from Eq. (5.5):

$$
\begin{aligned}
Z_q^{\rm RI'}((2\,{\rm GeV})^2, g^2_{\rm bare}) &= 0.805(14) - 0.336(6)(^{+0.002}_{-0.042})\\
&\quad \times (g^2_{\rm bare} - 1.5)\ \ [{\rm CM}].
\end{aligned}
\tag{5.11}
$$

The results obtained from the perturbative hypercubic correction, Table VII, have not been used in the final estimate (because we did not compute them for all $\beta's$), but they fall within the bounds at less than one sigma.

Finally, two lines in the lhs plot of Fig. 7 show the results for $g^2\langle A^2\rangle$ obtained from those in Table 3 of Ref. [7]:

$$
g^2\langle A^2\rangle_{10{\rm GeV}} = \begin{cases} 4.1 \pm 1.5\ {\rm GeV}^2 & \text{leading log} \\ 2.5 \pm 0.9\ {\rm GeV}^2 & \mathcal{O}(\alpha^4) \end{cases}. \tag{5.12}
$$

These values in Eq. (5.12) come from a totally different quantity: they have been extracted from the running of the ghost-gluon coupling constant. The results of Ref. [7] were obtained by applying an OPE formula including a Wilson coefficient approximated at the leading logarithm and at the order $\mathcal{O}(\alpha^4)$ but expanded in terms of α_T. Then, in order to be properly compared with the results of this work,

the values of Eq. (5.12) incorporate the correction by the effect of expanding the OPE formula in terms of the running coupling in $\overline{\text{MS}}$. The lattice spacing applied in Ref. [7] to get a physical scale, $a(3.9) = 0.0801$ fm, was also slightly smaller than the one used in this work (see, for instance, Table I), and this has been also taken into account in obtaining Eq. (5.12).

As a matter of fact, Eq. (5.12) exhibits a slower convergence of the perturbative series of the Wilson coefficient as in the present paper. From Tables III, IV, VI, and VIII, we see that the $O(\alpha^4)$ estimate is about 20% below the tree level while in Table 3 of [7], it is about 45% below the leading logarithm one. The two estimates agree rather well within the present accuracy.

G. Conversion to $\overline{\text{MS}}$

The conversion to $\overline{\text{MS}}$ can also be performed from Z_q^{pert} or $Z_q^{\text{RI}'}$ which contains a nonperturbative contribution. Usually, in the literature, the values are assumed to be perturbative. The conversion of Z_q^{pert} into $\overline{\text{MS}}$ will use the standard perturbative conversion formulae [13]. We get

$$Z_q^{\overline{\text{MS}}\,\text{pert}}((2\,\text{GeV})^2, g^2_{\text{bare}})/Z_q^{\text{pert}}((2\text{GeV})^2, g^2_{\text{bare}}) = 0.97,$$
$$Z_q^{\overline{\text{MS}}\,\text{pert}}((2\,\text{GeV})^2, g^2_{\text{bare}}) = 0.750(3)(7) - 0.313(20) \times (g^2_{\text{bare}} - 1.5). \quad (5.13)$$

The central value of this result is about 2% systematically below the results of [28]. Presumably, this can be interpreted as a small systematic correction due to our subtraction of the nonperturbative contribution in obtaining Z_q^{pert} in the RI'-MOM scheme and converting it to $Z_q^{\overline{\text{MS}}\,\text{pert}}$ at 2 GeV.

From Eq. (A24), it is easy to see how to include the $g^2\langle A^2\rangle$ nonperturbative contribution. Up to now, we have applied the result of the Appendix using RI'-MOM for the perturbative part and $\overline{\text{MS}}$ for the ratio in the corrective parenthesis. Had we wished to use the $\overline{\text{MS}}$ scheme for the perturbative contribution, we would have the main inconvenience of not knowing the OPE contribution for Z_q defined in the $\overline{\text{MS}}$ scheme. However, only with the aim of roughly estimating the nonperturbative correction, we can assume the OPE corrective parentheses to remain the same and then get

$$Z_q^{\overline{\text{MS}}\,\text{non}-\text{pert}}((2\,\text{GeV})^2, g^2_{\text{bare}}) = 0.781(6)(21) - 0.326(21) \times (g^2_{\text{bare}} - 1.5). \quad (5.14)$$

Notice that the nonperturbative contribution is about 4% at 2 GeV. Nevertheless, the results of [28] have been obtained at momenta larger than 2 GeV. Although their estimates and our $Z_q^{\text{RI}'}$ may agree with each other, a subtraction of the nonperturbative contribution in obtaining Z_q^{pert}, probably still required at the fitting window of [28] but not applied, could explain the small discrepancy of about 2% that we discussed above. The discrepancy is anyhow affecting only the conversion of $Z_q^{\text{RI}'}$ to $Z_q^{\overline{\text{MS}}\,\text{pert}}$ at 2 GeV. In Table 6 of [28], one finds results for $Z_q^{\overline{\text{MS}}}$ obtained at 2 GeV by applying the standard perturbative conversion formulae [13]. Indeed, as can be seen in Table IX, they turn out to fall between our results in Eqs. (5.13) and (5.14).

TABLE IX. Comparison of $Z_q^{\overline{\text{MS}}}(2\text{ GeV})$ given by Eqs. (5.13) and (5.14), and taken by Ref. [28] for $\beta = 3.9, 4.05$.

β	$Z_q^{\overline{\text{MS}}\,\text{pert}}(2\text{ GeV})$ by Eq. (5.13)	$Z_q^{\overline{\text{MS}}}(2\text{GeV})$ in [28]	$Z_q^{\overline{\text{MS}}\,\text{nonpert}}(2\text{ GeV})$ by Eq. (5.14)
3.9	0.738(8)	0.751(4)	0.769(22)
4.05	0.756(8)	0.780(5)	0.787(22)

H. Comparison of different estimates for the gluon condensate

Let us now compare the present estimate of $g^2\langle A^2\rangle$ to previous ones at $N_f = 2$ and $N_f = 0$, all taken at the renormalization scale of 10 GeV and, when needed, transformed to the very precise renormalization scheme for the OPE expansion defined in the Appendix.

In [4], a quenched study of Z_q using Wilson-Clover and overlap fermions ended with values of $\langle A^2\rangle_{\text{MOM}}$ in the range 2.67–3.2 GeV^2 with typical errors of 0.3 GeV^2. Notice that this computation was performed only up to leading logarithm for the Wilson coefficient and that the choice was to expand the perturbative series in terms of the coupling renormalized in the MOM scheme. (This is why we use the label MOM for the VEV.) Then, we can apply the expressions derived in the Appendix to obtain the estimates for $g^2\langle A^2\rangle$ in the above-mentioned renormalization scheme appearing in Table X. However, it is advocated in [4] that the $1/p^2$ contribution only increases by 10% when going from MOM to $\overline{\text{MS}}$. On the other hand, we have seen that between tree level and three loops, a decrease of 20% was observed. In [4], an artefact $\propto a/p^2$ was observed. We do not see it in the present analysis since the scaling of $g^2\langle A^2\rangle$ as a function of the lattice spacing indicates no visible $1/p^2$ contribution dependent on a.

In [6], a summary was performed of different estimates of $g^2\langle A^2\rangle$ from gluonic quantities at $N_f = 0$: α_s from the three-gluon vertex with equal momenta on the three legs (symmetric) and from the three-gluon vertex with one vanishing momentum (asymmetric), the ratio between the ghost and gluon propagators, and α_s from the ghost and gluon propagators, using Taylor's theorem. The ones involving gluon and ghost propagators agree fairly well, but the latter is the most accurate. It gives $g^2_T\langle A^2\rangle = 5.1^{+0.7}_{-1.1}$, although the applied OPE formula was obtained by expanding the involved perturbative series in terms of α_T. After the appropriate transformation, one obtains the results shown in Table X. We also quote in the table the estimate of $g^2\langle A^2\rangle$ from the symmetric three-gluon vertex,

TABLE X. Comparison of estimates of $g^2\langle A^2\rangle$ from different quantities at $N_f = 0$ and $N_f = 2$. All are taken at the scale $\mu = 10$ GeV. LL means leading logarithm for the Wilson coefficient. $O(\alpha^4)$ refers to the Chetyrkin and Maier computation.

		Measurement (GeV^2)		
N_f	Order $g^2\langle A^2\rangle$	Z_q	α_T	3-gluon
0	LL	9.4(3)	5.2(1.1)	10(3)
	$O(\alpha^4)$	9.0(3)	3.7(8)	
2	LL	2.7(4)	4.1(1.5)	
	$O(\alpha^4)$	2.55(36)	2.5(9)	

more precise than the one coming from the asymmetric vertex, and that appeared to be much higher than the estimate from α_T and compatible with that from the quark propagator. In the case of the three-gluon estimates, no available $O(\alpha^4)$ Wilson coefficient can help us to go beyond the leading logarithm approximation. However, comparing the leading logarithm estimates of the ones approximated at the order $O(\alpha^4)$, a clear discrepancy (by a factor of about two) appears between the estimates from ghost and gluon propagators and those from vertices or the quark propagator. This discrepancy could imply that some systematic uncertainty is not completely under control. One might, for instance, guess that $1/p^4$- contributions can be invoked to reduce that discrepancy. For this to happen, the $1/p^4$ contributions had to be negative, and had to tend to increase the estimate of $g^2\langle A^2\rangle$, for the OPE formula of α_T, while it had to be positive, and reduce $g^2\langle A^2\rangle$, for the quark propagator. Indeed, although no stable fit including $1/p^4$ contributions can be performed, the sign seems to be the right one for α_T in [7]. Also the right sign of the contributions to Z_q is found in Ref. [4].

In [7], the strong coupling constant was computed along lines similar to what is done here, on the same set of ETMC gauge configurations with $N_f = 2$. The necessity of a nonperturbative $\propto 1/p^2$ contribution was also found and the resulting condensate, $g^2\langle A^2\rangle_{10\ \mathrm{GeV}} = 2.3(8)$, obtained through an OPE formula approximated at the $O(\alpha^4)$ order and expanded in α_T, can be properly transformed[6] to give the value of Table X, also quoted in Eq. (5.12), which agrees strikingly well with the result of Table VIII (the one we also quote in Table X) or that of Eq. (5.10). The value obtained through a leading-logarithm-approximated formula is also displayed in Table X. In [10], Martinelli and Sachrajda proposed a criterion to validate the use of operator expansion which we apply in this paper. They concluded that one should compare the difference of the highest order of the perturbative expansion for two different quantities with the nonperturbative contribution and check that the former is small compared to the latter. We have compared the highest order of the perturbative expansion of Z_q with the $1/p^2$ contribution and find that the ratio ranges between $1/10$ and $1/3$, depending on the momentum. This is a good indication of the validity of our use of the operator expansion. Had we used the perturbative expansion only up to $O(\alpha)$, this criterion would not have been fulfilled.

Furthermore, all these estimates in Table X show a clear tendency of a decrease of $g^2\langle A^2\rangle$ from $N_f = 0$ to $N_f = 2$. This might support an interpretation of $g^2\langle A^2\rangle$ as originating in instantons [29], since the instanton density should decrease with light dynamical masses.

[6]We have taken into account the different lattice spacing in [7].

VI. CONCLUSION

We have studied with care the twisted quark propagators produced on the ETMC set of $N_f = 2$ gauge configurations. Our goal was to concentrate on two major issues: the correction for lattice spacing artefacts, particularly the hypercubic ones, and the presence of a sizeable nonperturbative contribution of the A^2 operator. The latter is expected to be sizeable because it was seen in the quenched case [4] and in the unquenched study of the strong coupling constant [7], and since the Wilson coefficient of $g^2\langle A^2\rangle$ is not small in Z_q [9]. This is an important issue since, from our estimates, it gives an $\sim$4% contribution at 2 GeV. A reliable estimate of this nonperturbative correction needs a large enough fitting range, which allows us to distinguish a $1/p^2$ contribution from perturbative logarithms. But the fitting window is restricted below by infrared effects and above by lattice spacing artefacts. We thus need to improve our control on dominant lattice spacing artefacts which are of two types: hypercubic ones and $\propto a^2p^2$ ones.

Concerning the hypercubic artefacts, we have summarized the nonperturbative correcting method [24,25] which we compared systematically with the perturbative results of [26]. Z_q has very large hypercubic artefacts which display, as a function of p^2, a half-fishbone very far from a smooth curve (see Fig. 1). We check carefully how these fishbones are ''swallowed'' by the corrective methods. It is worthwhile to emphasize that the democratic method, prescribing, for instance, a cut on $p^{[4]}/p^2$ to drastically reduce the number of allowed hypercubic orbits, is not good enough to eliminate the fishbones and to leave us with a smooth curve for Z_q.

The perturbative method to correct hypercubic artefacts suffers from some options left: what to take for the coupling constant, use of p_μ or $\tilde{p}_\mu = a^{-1}\sin(ap_\mu)$? We first tried to stick to the prescription of [26] and use the boosted coupling constant. This reduces the hypercubic artefacts only up to $a^2p^2 \simeq 1.6$ (see Fig. 2, lhs). Guided by the test on the fishbone reduction, we then propose a prescription based on the same perturbative formulae but using p_μ. For Z_q, this reduces the hypercubic artefacts up to $a^2p^2 \simeq 3.5$ which has been our upper bound in this work (see Fig. 2, rhs).

We test also the nonperturbative method to correct hypercubic artefacts. We use two prescriptions. The first one

uses a sliding window and the second one uses only one fitting window on the full momentum range.

We find that the hypercubic artefacts are sufficiently well described and cured by two terms: $\propto a^2 p^{[4]}/p^2$ and $\propto a^4 p^{[4]}$. We fit the coefficients of these quantities and check their scaling with β.

From the resulting hypercubic corrected function $Z_q(a^2p^2, a^2\Lambda^2_{\rm QCD})$ we perform fits which incorporate the perturbative running, a nonperturbative $1/p^2$ term, presumably related to $g^2\langle A^2\rangle$ through the Wilson expansion, and a hypercubic insensitive lattice spacing artefact proportional to a^2p^2. This local operator A^2 should be properly renormalized and, as will be explained in the Appendix, we choose the $\overline{\rm MS}$ scheme for the renormalization procedure and thus obtain Eq. (5.5). The fits are good. The a^2p^2 term scales almost perfectly in lattice units, as expected. The $g^2\langle A^2\rangle$ term also scales rather well in physical units, as expected. The accuracy on $g^2\langle A^2\rangle$ is reduced by some correlations in the fits: we see a correlation between the method used to correct hypercubic artefacts and the estimated value of $g^2\langle A^2\rangle$. We also see a correlation between the fitting range and the resulting $g^2\langle A^2\rangle$. But all values of $g^2\langle A^2\rangle$ fall into the same ballpark and none of these fits can be made without such a positive contribution. To estimate the systematic uncertainty, we have considered a large panel of fitting methods, all at more than four sigmas from zero, except at $\beta = 4.2$ with the sliding window, where they are only 2.5 sigmas above zero. Comparing the fitted $\langle A^2\rangle$ using the tree level Wilson coefficient and that using the three loops one, we find that the latter is about 20% below the former.

The perturbative contribution to Z_q, $Z_q^{\rm pert}$ has a linear dependence in the bare lattice coupling: see Fig. 8 and Eq. (5.10), as expected from perturbation theory, but with a larger coefficient, even when the boosted coupling constant is used in perturbation theory.

We also merge all three β's after having subtracted the a^2p^2 term and rescaled the $\beta = 4.05, 4.2$ to 3.9, using the ratios of $Z_q^{\rm pert}(\mu)$. The overlap of the three data sets is rather good. The need of a nonperturbative contribution is also visible there. Both perturbative and nonperturbative contributions decrease with the momentum and are convex. This makes the separation difficult. Grossly speaking, they share the decrease between 4 and 40 GeV^2 in equal parts.

We have converted our results for $Z_q^{\rm RI'}$ and its perturbative part $Z_q^{\rm pert}(\mu)$ into the $\overline{\rm MS}$ scheme.

Combining all the results, we find, using the three loop Wilson coefficient:

$$
\begin{aligned}
&g^2(\mu^2)\langle A^2\rangle_{\mu^2 CM} = 2.01(11)(^{+0.61}_{-0.73})\text{GeV}^2 \mu = 10\ \text{GeV},\\
&Z_q^{\rm pert}((2\text{GeV})^2, g^2_{\rm bare}) = 0.773(3)(7) - 0.323(6)(^{+0.002}_{-0.040})(g^2_{\rm bare} - 1.5),\\
&Z_q^{\rm RI'}((2\ \text{GeV})^2, g^2_{\rm bare}) = 0.805(14) - 0.336(6)(^{+0.002}_{-0.040})(g^2_{\rm bare} - 1.5),\\
&Z_q^{\overline{\rm MS}\ \rm pert}((2\ \text{GeV})^2, g^2_{\rm bare}) = 0.750(3)(7) - 0.313(20)(g^2_{\rm bare} - 1.5),\\
&Z_q^{\overline{\rm MS}\ \rm nonperturbative}((2\ \text{GeV})^2, g^2_{\rm bare}) = 0.781(6)(21) - 0.326(21)(g^2_{\rm bare} - 1.5),
\end{aligned}
\tag{6.1}
$$

where the systematic error is estimated from the scattering of the results in Tables III, IV, VI, and VIII. We use the lattice spacings listed in Table I.

Furthermore, Table X also shows a nice agreement between the condensates for $N_f = 2$, although some systematics appear not to be under control for $N_f = 0$. This supports the interpretation of the $\propto 1/p^2$ contribution as being due to a condensate of the only dimension-two operator in Landau gauge: A^2. Another confirmation comes from the validity of Martinelli-Sachrajda's criterion [10]. The accuracy on $g^2\langle A^2\rangle$ is limited, however, due to several correlations in the fits. Further and more accurate checks of the consistency of $g^2\langle A^2\rangle$ from other renormalization constants will be very welcome.

ACKNOWLEDGMENTS

We thank Alain Le Yaouanc, Vittorio Lubicz, and Gian-Carlo Rossi for a critical reading of this manuscript and the very useful subsequent discussions. This work was granted access to the HPC resources of CINES and IDRIS under Allocation No. 2010-052271 made by GENCI. J. R.-Q. is indebted to the Spanish MICINN for support by Research Project No. FPA2009-10773 and to "Junta de Andalucia" for support by Project No. P07FQM02962. Z. Liu thanks the UK Science and Technology Facilities Council (STFC) for financial support.

APPENDIX: THE WILSON COEFFICIENTS AT $O(\alpha^4)$

The purpose of this Appendix is to describe briefly the OPE analysis of the quark propagator renormalization constant defined in Eq. (1.2) that leads us to Eq. (5.1), where the four-loops results in Ref. [9] are exploited to derive the Wilson coefficients with the appropriate renormalization prescription. This OPE analysis is analogous to the one performed in Refs. [2,3,5,6]. The starting point is the OPE of the inverse of the quark propagator:

$$
\begin{aligned}
&S^{-1}(p^2,\mu^2)\\
&\quad = Z_q^{-1}(\mu^2)S_{\rm bare}^{-1}(p^2)\\
&\quad = (S^{\rm pert})^{-1}(p^2,\mu^2) + i\not{p}\frac{c_{2Z_q}(\frac{p^2}{\mu^2},\alpha(\mu))}{p^2}\frac{\langle A^2\rangle_{R,\mu^2}}{4(N_c^2-1)}\\
&\quad = \frac{(S^{\rm pert}_{\rm bare})^{-1}(p^2)}{Z_q^{\rm pert}(\mu^2)} + i\not{p}\frac{c_{2Z_q}(\frac{p^2}{\mu^2},\alpha(\mu))}{p^2}\frac{\langle A^2\rangle_{R,\mu^2}}{4(N_c^2-1)},
\end{aligned}
\tag{A1}
$$

where only the leading term in $\not{p}$ is kept, the quark mass being assumed to be negligible or to vanish. The cutoff regularization dependence is omitted for the bare quantities, but that on the renormalization momentum, μ, is explicitly written for the renormalized ones. In the RI'-MOM scheme, we define $Z_q^{\rm RI'}$ such that $(S_{\rm bare})^{-1}(p^2) = i\not{p}\delta_{ab}Z_q^{\rm RI'}(p^2)$ and $Z_q^{\rm pertRI'}$ such that $(S^{\rm pert}_{\rm bare})^{-1}\times(p^2) = i\not{p}\delta_{ab}Z_q^{\rm pertRI'}(p^2)$. Then, the renormalization momentum, μ^2, taken to lie on the perturbative regime, one can apply Eq. (1.2) and obtain

$$
\begin{aligned}
\frac{Z_q^{RI'}(p^2)}{Z_q^{\rm pert}(\mu^2)} &= \frac{Z_q^{\rm pertRI'}(p^2)}{Z_q^{\rm pert}(\mu^2)} + c_{2Z_q}\left(\frac{p^2}{\mu^2},\alpha(\mu)\right)\frac{\langle A^2\rangle_{R,\mu^2}}{4(N_c^2-1)p^2}\\
&= c_{0Z_q}\left(\frac{p^2}{\mu^2},\alpha(\mu)\right) + c_{2Z_q}\left(\frac{p^2}{\mu^2},\alpha(\mu)\right)\\
&\quad\times\frac{\langle A^2\rangle_{R,\mu^2}}{4(N_c^2-1)p^2},
\end{aligned}
\tag{A2}
$$

which implies a definition of c_{0Z_q} and where $c_{2Z_q}(p^2,\mu^2)$ is the Wilson coefficient of $g^2\langle A^2\rangle$. Although not yet specifying the renormalization scheme of $Z_q^{\rm pert}(\mu^2)$, we know that

$$
c_{0Z_q}(1,\alpha(\mu)) = 1 + O(\alpha^2), \tag{A3}
$$

while c_{2Z_q} is known up to $O(\alpha^4)$ in the $\overline{\rm MS}$ scheme [9] and, in particular, $c_{2Z_q}^{\overline{\rm MS}}(1,\alpha(\mu))$ is given in Eq. (18) of that paper using $q^2=\mu^2$. Let us keep in mind, however, that

$$
\begin{aligned}
c_{2Z_q}(1,\alpha(\mu)) &= \frac{32\pi}{3}\alpha(\mu)(1+\mathcal{O}(\alpha(\mu)))\\
&= \frac{8g^2(\mu)}{3}(1+\mathcal{O}(\alpha(\mu))).
\end{aligned}
\tag{A4}
$$

Now, with the help of the appropriate renormalization constants, one can also write Eq. (A2) in terms of bare quantities:

$$
\begin{aligned}
Z_q^{RI'}(p^2) &= Z_q^{\rm pert}(\mu^2)c_{0Z_q}\left(\frac{p^2}{\mu^2},\alpha(\mu)\right)\\
&\quad + Z_q^{\rm pert}(\mu^2)Z_{A^2}^{-1}(\mu^2,\Lambda^2)c_{2Z_q}\left(\frac{p^2}{\mu^2},\alpha(\mu)\right)\\
&\quad\times\frac{\langle A^2\rangle}{4(N_c^2-1)p^2},
\end{aligned}
\tag{A5}
$$

where $A_R^2 = Z_{A^2}^{-1}A^2$. Then, as the μ-dependence of both the lhs and rhs of Eq. (A5) should match each other for any p, one can take the logarithmic derivative with respect to μ and the infinite cutoff limit, term by term, on the rhs and obtain:

$$
\begin{aligned}
&\gamma_q(\alpha(\mu)) + \left\{\frac{\partial}{\partial\log\mu^2} + \beta(\alpha(\mu))\frac{\partial}{\partial\alpha}\right\}\ln c_{0Z_q}\left(\frac{q^2}{\mu^2},\alpha(\mu)\right) = 0,\\
&-\gamma_{A^2}(\alpha(\mu)) + \gamma_q(\alpha(\mu)) + \left\{\frac{\partial}{\partial\log\mu^2} + \beta(\alpha(\mu))\frac{\partial}{\partial\alpha}\right\}\\
&\quad\times\ln c_{2Z_q}\left(\frac{q^2}{\mu^2},\alpha(\mu)\right) = 0,
\end{aligned}
\tag{A6}
$$

where the β-function, chosen to be in $\overline{\rm MS}$, is defined as

$$
\beta(\alpha(\mu)) = \frac{d}{d\log\mu^2}\alpha(\mu) = -4\pi\sum_{i=0}\beta_i\left(\frac{\alpha(\mu)}{4\pi}\right)^{i+2} \tag{A7}
$$

and where $\gamma_q(\alpha(\mu))$ and $\gamma_{A^2}(\alpha(\mu))$ are the anomalous dimensions for the fermion propagator and local operator A^2, respectively, which are formally defined as

$$
\gamma_X(\alpha(\mu)) = \frac{d}{d\log\mu^2}\log Z_X = -\sum_{i=0}\gamma_i^X\left(\frac{\alpha(\mu)}{4\pi}\right)^{i+1}, \tag{A8}
$$

where X stands for q or A^2. The scheme for the anomalous dimension of Z_{A^2} is imposed through the renormalization of the local operator A^2, as was done in Ref. [2] to obtain its leading logarithm contribution, and it is only known in the $\overline{\rm MS}$ at the order $\mathcal{O}(\alpha^4)$ [30]. Then that is the only possible choice of scheme for γ_{A^2} in Eqs. (A6). Concerning $Z_q^{\rm pert}$, its scheme is determined by the renormalization prescription for the nonperturbative propagator in the left-hand-side of Eq. (A1). Both $\overline{\rm MS}$ and RI'-MOM are possible. Our aim is to obtain a nonperturbative formula to confront the lattice estimate of the RI'-MOM quark renormalization constant, and it is thus convenient also to prescribe the RI'-MOM scheme for $Z_q^{\rm pert}$. Thus, Eqs. (A6) must be rewritten as

$$
\begin{aligned}
&\gamma_q^{\rm RI'}(\alpha(\mu)) + \left\{\frac{\partial}{\partial\log\mu^2} + \beta(\alpha(\mu))\frac{\partial}{\partial\alpha}\right\}\ln c_{0Z_q}^{\rm RI'}\left(\frac{q^2}{\mu^2},\alpha(\mu)\right) = 0,\\
&-\gamma_{A^2}^{\overline{\rm MS}}(\alpha(\mu)) + \gamma_q^{\rm RI'}(\alpha(\mu)) + \left\{\frac{\partial}{\partial\log\mu^2} + \beta(\alpha(\mu))\frac{\partial}{\partial\alpha}\right\}\\
&\quad\times\ln c_{2Z_q}^{\rm W\overline{MS}}\left(\frac{q^2}{\mu^2},\alpha(\mu)\right) = 0,
\end{aligned}
\tag{A9}
$$

where

$$
c_{0Z_q}^{\rm RI'}\left(\frac{p^2}{\mu^2},\alpha(\mu)\right) \equiv \frac{Z_q^{\rm pertRI'}(p^2)}{Z_q^{\rm pertRI'}(\mu^2)} \tag{A10}
$$

and $c_{2Z_q}^{\rm W\overline{MS}}$ is in the W$\overline{\rm MS}$ scheme,[7] explicitly defined by the second equation of (A9), after the RI'-MOM prescription for $Z_q^{\rm pert}$, that of $\overline{\rm MS}$ for A^2, and by the choice of a boundary

[7] We define this scheme by imposing that the local operator of the Wilson expansion be renormalized in $\overline{\rm MS}$, while the expanded operator (the quark propagator, in our case) is in an MOM scheme. We called this "Wilson $\overline{\rm MS}$."

condition, $c_{2Z_q}^{\mathrm{W}\overline{\mathrm{MS}}}(1,\alpha(q))$. Then, from Eq. (A2), one obtains

$$Z_q^{\mathrm{RI}'}(p^2) = Z_q^{\mathrm{pertRI}'}(\mu^2) c_{0Z_q}^{\mathrm{RI}'}\left(\frac{p^2}{\mu^2},\alpha(\mu)\right) \times\left(1+\frac{c_{2Z_q}^{\mathrm{W}\overline{\mathrm{MS}}}(\frac{p^2}{\mu^2},\alpha(\mu))}{c_{0Z_q}^{\mathrm{RI}'}(\frac{p^2}{\mu^2},\alpha(\mu))}\frac{\langle A^2\rangle_{R,\mu^2}}{4(N_c^2-1)p^2}\right), \quad \text{(A11)}$$

and, in practice, both Eqs. (A9) can be combined to give the following differential equation:

$$\left\{-\gamma_{A^2}^{\overline{\mathrm{MS}}}(\alpha(\mu)) + \frac{\partial}{\partial\log\mu^2} + \beta(\alpha(\mu))\frac{\partial}{\partial\alpha}\right\} \times \frac{c_{2Z_q}^{\mathrm{W}\overline{\mathrm{MS}}}(\frac{p^2}{\mu^2},\alpha(\mu))}{c_{0Z_q}^{\mathrm{RI}'}(\frac{p^2}{\mu^2},\alpha(\mu))} = 0, \quad \text{(A12)}$$

that can be solved to provide us with the ratio of Wilson coefficients, c_{2Z_q}/c_{0Z_q}, required to implement Eq. (A11). For the purpose of the best comparison with the results from the analysis performed in Ref. [6], we applied

$$c_{2Z_q}^{\mathrm{W}\overline{\mathrm{MS}}}(1,\alpha(p)) \equiv c_{2Z_q}^{\overline{\mathrm{MS}}}(1,\alpha(p)), \quad \text{(A13)}$$

where $c_{2Z_q}^{\overline{\mathrm{MS}}}(1,\alpha(\mu))$ is taken from Eq. (18) of Ref. [9] using $q^2=\mu^2$ as a boundary condition which is equivalent to the one applied in the analysis of Ref. [6].

On the other hand, if we take Z_q^{pert} to be renormalized in $\overline{\mathrm{MS}}$, the equations in (A6) read

$$\begin{aligned}&\gamma_q^{\overline{\mathrm{MS}}}(\alpha(\mu)) + \left\{\frac{\partial}{\partial\log\mu^2} + \beta(\alpha(\mu))\frac{\partial}{\partial\alpha}\right\} \times \ln c_{0Z_q}^{\overline{\mathrm{MS}}}\left(\frac{q^2}{\mu^2},\alpha(\mu)\right) = 0,\\ &-\gamma_{A^2}^{\overline{\mathrm{MS}}}(\alpha(\mu)) + \gamma_q^{\overline{\mathrm{MS}}}(\alpha(\mu)) + \left\{\frac{\partial}{\partial\log\mu^2} + \beta(\alpha(\mu))\frac{\partial}{\partial\alpha}\right\} \times \ln c_{2Z_q}^{\overline{\mathrm{MS}}}\left(\frac{q^2}{\mu^2},\alpha(\mu)\right) = 0, \quad \text{(A14)}\end{aligned}$$

where $c_{2Z_q}^{\overline{\mathrm{MS}}}$ is the Wilson coefficient computed in Ref. [9], provided that the boundary condition, $c_{2Z_q}^{\overline{\mathrm{MS}}}(1,\alpha(\mu))$, is taken again from Eq. (18) of the same paper using $q^2=\mu^2$. Then we can again combine Eqs. (A14) to obtain, for $c_2^{\overline{\mathrm{MS}}}/c_0^{\overline{\mathrm{MS}}}$, the same equation Eq. (A12) that, with the same boundary condition, leads to

$$\frac{c_{2Z_q}^{\mathrm{W}\overline{\mathrm{MS}}}(\frac{p^2}{\mu^2},\alpha(\mu))}{c_{0Z_q}^{\mathrm{RI}'}(\frac{p^2}{\mu^2},\alpha(\mu))} = \frac{c_{2Z_q}^{\overline{\mathrm{MS}}}(\frac{p^2}{\mu^2},\alpha(\mu))}{c_{0Z_q}^{\overline{\mathrm{MS}}}(\frac{p^2}{\mu^2},\alpha(\mu))}. \quad \text{(A15)}$$

On the other hand, we can also combine the second equation of (A9) with the second one of Eq. (A14) and obtain

$$\left\{\gamma_q^{\mathrm{RI}'}(\alpha(\mu)) - \gamma_q^{\overline{\mathrm{MS}}}(\alpha(\mu)) + \frac{\partial}{\partial\log\mu^2} + \beta(\alpha(\mu))\frac{\partial}{\partial\alpha}\right\} \times \frac{c_{2Z_q}^{\mathrm{W}\overline{\mathrm{MS}}}(\frac{p^2}{\mu^2},\alpha(\mu))}{c_{2Z_q}^{\overline{\mathrm{MS}}}(\frac{p^2}{\mu^2},\alpha(\mu))} = 0, \quad \text{(A16)}$$

that, according to Eq. (A13), can be solved with the boundary condition $c_{2Z_q}^{\overline{\mathrm{MS}}}(1,\alpha(p))/c_{2Z_q}^{\overline{\mathrm{MS}}}(1,\alpha(p)) \equiv 1$ and leaves us with a relation of $\mathrm{W}\overline{\mathrm{MS}}$ and $\overline{\mathrm{MS}}$ Wilson coefficients which allows Eq. (A11) to be rewritten as

$$Z_q^{\mathrm{RI}'}(p^2) = Z_q^{\mathrm{pertRI}'}(\mu^2) c_{0Z_q}^{\mathrm{RI}'}\left(\frac{p^2}{\mu^2},\alpha(\mu)\right) \times\left(1+\frac{c_{2Z_q}^{\overline{\mathrm{MS}}}(\frac{p^2}{\mu^2},\alpha(\mu))}{c_{0Z_q}^{\mathrm{RI}'}(\frac{p^2}{\mu^2},\alpha(\mu))}\frac{c_{2Z_q}^{\mathrm{W}\overline{\mathrm{MS}}}(\frac{p^2}{\mu^2},\alpha(\mu))}{c_{2Z_q}^{\overline{\mathrm{MS}}}(\frac{p^2}{\mu^2},\alpha(\mu))} \times\frac{\langle A^2\rangle_{\overline{\mathrm{MS}},\mu^2}}{4(N_c^2-1)p^2}\right), \quad \text{(A17)}$$

where, furthermore, $c_{2Z_q}^{\overline{\mathrm{MS}}}$ is to be taken from Ref. [9] and $c_{0Z_q}^{\mathrm{RI}'}$ from Ref. [13]. Thus we can use either Eq. (A11) with the solution of Eq. (A9) or Eq. (A17) with that of Eq. (A16) to confront the lattice estimates of $Z_q^{\mathrm{RI}'}$. Both expressions are equivalent. In the first case, one can proceed as was done in Ref. [7] to solve Eq. (A9). To illustrate this first method, let us remind the reader that Eq. (A9) can be solved at the leading logarithm by applying the following ansatz,

$$\frac{c_{2Z_q}^{\mathrm{W}\overline{\mathrm{MS}}}(\frac{p^2}{\mu^2},\alpha(\mu))}{c_{0Z_q}^{\mathrm{RI}'}(\frac{p^2}{\mu^2},\alpha(\mu))} = \frac{32\pi}{3}\alpha(p)\left(\frac{\alpha(\mu)}{\alpha(p)}\right)^a(1+\mathcal{O}(\alpha)), \quad \text{(A18)}$$

where we apply Eq. (A4), and the exponent a, required to satisfy Eq. (A9), should be

$$a = \frac{\gamma_0^{A^2}}{\beta_0} = \frac{105-8N_f}{132-8N_f}. \quad \text{(A19)}$$

In the second case, to solve Eq. (A16), a similar ansatz extended to three-loops order can be applied,

$$\frac{c_{2Z_q}^{\mathrm{W}\overline{\mathrm{MS}}}(\frac{p^2}{\mu^2},\alpha(\mu))}{c_{2Z_q}^{\overline{\mathrm{MS}}}(\frac{p^2}{\mu^2},\alpha(\mu))} = \left(\frac{\alpha(\mu)}{\alpha(p)}\right)^b\left(\frac{1+\sum_i r_i(\frac{\alpha(\mu)}{4\pi})^i}{1+\sum_i r_i(\frac{\alpha(p)}{4\pi})^i}\right), \quad \text{(A20)}$$

where we use Eq. (A13) for the boundary condition. Then, by requiring that the ansatz Eq. (A20) verifies Eq. (A16), the coefficients b and r_i will be obtained in terms of those for the fermion propagator $\overline{\mathrm{MS}}$ and RI'-MOM anomalous dimensions and for the $\overline{\mathrm{MS}}$ β-function. However, in this case,

$$b = \frac{\gamma_0^{q\overline{\mathrm{MS}}} - \gamma_0^{q\mathrm{RI}'}}{\beta_0} = 0, \tag{A21}$$

because the first-loop coefficient for the anomalous dimension is scheme independent. (In the particular Landau gauge, this scheme-independent first-loop coefficient is also zero for any scheme [13].) Furthermore, as can be seen in Appendix C of Ref. [13], one is also left with $\gamma_1^{q\overline{\mathrm{MS}}} \equiv \gamma_1^{q\mathrm{RI}'}$ in the Landau gauge. Then,

$$r_1 = \frac{\gamma_1^{q\overline{\mathrm{MS}}} - \gamma_1^{q\mathrm{RI}'}}{\beta_0} = 0, \tag{A22}$$

and the Wilson coefficients for $\overline{\mathrm{MS}}$ and RI'-MOM will thus differ only at the order $\mathcal{O}(\alpha^2)$, with the nonzero r_i's coefficients to be applied in Eq. (A20) given by

$$r_2 = \frac{\gamma_2^{q\overline{\mathrm{MS}}} - \gamma_2^{q\mathrm{RI}'}}{2\beta_0} = -25.4642 + 2.3333N_f,$$
$$r_3 = \frac{\gamma_3^{q\overline{\mathrm{MS}}} - \gamma_3^{q\mathrm{RI}'}}{3\beta_0} - \beta_1 \frac{\gamma_2^{q\overline{\mathrm{MS}}} - \gamma_2^{q\mathrm{RI}'}}{3\beta_0^2}$$
$$= -1489.9796 + 246.4424N_f - 6.4609N_f^2, \tag{A23}$$

where the three- and four-loop coefficient in $\overline{\mathrm{MS}}$ and RI'-MOM for the fermion propagator anomalous dimension have again been obtained from Ref. [13]. This leads, using Eqs. (A17) and (A20)–(A23) with $N_c^2 - 1 = 8$ and $N_f = 2$, to our final formulae for the free-of-artefacts lattice determination of Z_q:

$$Z_q^{\text{Latt artefree}}(p^2, \beta) = Z_q^{\text{pertRI}'}(\mu'^2) c_{0Z_q}^{\mathrm{RI}'}\left(\frac{p^2}{\mu'^2}, \alpha(\mu')\right)\left(1 + \frac{c_{2Z_q}^{\overline{\mathrm{MS}}}(\frac{p^2}{\mu^2}, \alpha(\mu))}{c_{0Z_q}^{\mathrm{RI}'}(\frac{p^2}{\mu^2}, \alpha(\mu))} \frac{1 - 0.1317\alpha^2(\mu) - 0.5155\alpha^3(\mu)}{1 - 0.1317\alpha^2(p) - 0.5155\alpha^3(p)} \frac{\langle A^2\rangle_{\overline{\mathrm{MS}},\mu^2}}{32p^2}\right). \tag{A24}$$

In this last equation, we exploited the fact that the expression in parentheses in Eqs. (A17) and (A24) does not vary with the renormalization momentum for the local operator A^2, as can be inferred from Eq. (A12). Thus, once a given momentum, μ'^2, is fixed for the renormalization of the fermion propagator in the lhs of Eq. (A1), the one appearing in $Z_q^{\text{pertRI}'}$ in front of the expression in parentheses, one is still left with the freedom of choosing a renormalization momentum, μ^2, which does not need to be the same, for the local operator A^2 inside the parentheses.

In Eq. (A24), the coefficients $c_{0Z_q}^{RI'}$ and $c_{2Z_q}^{\overline{\mathrm{MS}}}$ are known from perturbation theory; the former can be obtained from Ref. [13] and the latter from Ref. [9]. Two parameters are to be fitted: $Z_q^{\text{pertRI}'}(\mu'^2)$ and the nonperturbative condensate $g^2(\mu)\langle A^2\rangle_{R,\mu^2}$. It is important to underline that *the condensate is defined via the OPE*, i.e., from Eqs. (A17) and (A24). Its precise definition depends on the renormalization scheme, the renormalization scale, as well as the order in perturbation theory to which the coefficients c_{0Z_q} and c_{2Z_q} are used. In Eqs. (A17) and (A24), the renormalization scheme for $g^2(\mu)\langle A^2\rangle_{R,\mu^2}$ is $\overline{\mathrm{MS}}$ and the scale is μ (10 GeV in our calculations). The coupling we use for the perturbative expansions of these coefficients, c_{0Z_q} and c_{2Z_q}, is also chosen to be the $\overline{\mathrm{MS}}$ one. These choices are kept all along in the present paper. If we now wish to compare $g^2(\mu)\langle A^2\rangle_{R,\mu^2}$ from the present calculation to that from another calculation, for example, from the strong coupling constant [7], *we must as far as possible use the same precise definition in both cases*. However, its dependence on the scheme and on the order in perturbation theory is not so important; as seen in Sec. V, other systematic uncertainties are larger.

[1] M. Lavelle and M. Oleszczuk, Mod. Phys. Lett. A **7**, 3617 (1992); J. Ahlbach, M. Lavelle, M. Schaden, and A. Streibl, Phys. Lett. B **275**, 124 (1992).

[2] P. Boucaud, A. Le Yaouanc, J. P. Leroy, J. Micheli, O. Pène, and J. Rodríguez-Quintero, Phys. Rev. D **63**, 114003 (2001).

[3] P. Boucaud, A. Le Yaouanc, J. P. Leroy, J. Micheli, O. Pène, and J. Rodríguez-Quintero, Phys. Lett. B **493**, 315 (2000); F. De Soto and J. Rodríguez-Quintero, Phys. Rev. D **64**, 114003 (2001).

[4] Ph. Boucaud *et al.*, Phys. Rev. D **74**, 034505 (2006).

[5] Ph. Boucaud *et al.*, J. High Energy Phys. 01 (2006) 037.

[6] Ph. Boucaud, F. De Soto, J. P. Leroy, A. Le Yaouanc, J. Micheli, O. Pène, and J. Rodríguez-Quintero, Phys. Rev. D **79**, 014508 (2009).

[7] B. Blossier, Ph. Boucaud, F. De soto, V. Morenas, M. Gravina, O. Pène, and J. Rodríguez-Quintero (ETM Collaboration), Phys. Rev. D **82**, 034510 (2010).
[8] E. Megias, E. Ruiz Arriola, and L. L. Salcedo, Phys. Rev. D **75**, 105019 (2007).
[9] K. G. Chetyrkin and A. Maier, J. High Energy Phys. 01 (2010), 092.
[10] G. Martinelli and C. T. Sachrajda, Nucl. Phys. **B478**, 660 (1996).
[11] F. V. Gubarev and V. I. Zakharov, Phys. Lett. B **501**, 28 (2001); K. G. Chetyrkin, S. Narison, and V. I. Zakharov, Nucl. Phys. **B550**, 353 (1999); D. Dudal, H. Verschelde, and S. P. Sorella, Phys. Lett. B **555**, 126 (2003); K. I. Kondo, Phys. Lett. B **572**, 210 (2003); Phys. Lett. B **514**, 335 (2001).
[12] P. Boucaud *et al.*, Phys. Lett. B **575**, 256 (2003).
[13] K. G. Chetyrkin and A. Retey, Nucl. Phys. **B583**, 3 (2000); K. G. Chetyrkin, Nucl. Phys. **B710**, 499 (2005); http://www-ttp.particle.uni-karlsruhe.de/Progdata/ttp99/ttp99-43/.
[14] R. Wilson, Phys. Rev. **179**, 1499 (1969).
[15] M. A. Shifman, A. I. Vainshtein, and V. I. Zakharov, Nucl. Phys. **B147**, 385 (1979); M. A. Shifman, A. I. Vainshtein, M. B. Voloshin, and V. I. Zakharov, Phys. Lett. **77B**, 80 (1978).
[16] P. Weisz, Nucl. Phys. **B212**, 1 (1983).
[17] R. Frezzotti, P. A. Grassi, S. Sint, and P. Weisz (Alpha Collaboration), J. High Energy Phys. 08 (2001) 058.
[18] Ph. Boucaud *et al.* (ETM Collaboration), Comput. Phys. Commun. **179**, 695 (2008).
[19] Ph. Boucaud *et al.* (ETM Collaboration), Phys. Lett. B **650**, 304 (2007).
[20] C. Urbach *et al.* (ETM Collaboration), Proc. Sci. LAT2007 (2007) 022 [arXiv:0710.1517].
[21] P. Dimopoulos *et al.* (ETM Collaboration), Proc. Sci. LATTICE2008 (2008) 103 [arXiv:0810.2873].
[22] R. Frezzotti and G. C. Rossi, J. High Energy Phys. 08 (2004) 007.
[23] R. Baron *et al.* (ETM Collaboration), J. High Energy Phys. 08 (2010) 097.
[24] D. Becirevic, Ph. Boucaud, J. P. Leroy, J. Micheli, O. Pène, J. Rodríguez-Quintero, and C. Roiesnel, Phys. Rev. D **60**, 094509 (1999).
[25] F. de Soto and C. Roiesnel, J. High Energy Phys. 09 (2007) 007.
[26] M. Constantinou, V. Lubicz, H. Panagopoulos, and F. Stylianou, J. High Energy Phys. 10 (2009) 064.
[27] S. Capitani, Phys. Rep. **382**, 113 (2003).
[28] M. Constantinou *et al.*, J. High Energy Phys. 08 (2010) 068.
[29] Ph. Boucaud *et al.*, Phys. Rev. D **66**, 034504 (2002).
[30] J. A. Gracey, Phys. Lett. B **552**, 101 (2003).